Environment International 190 (2024) 108891

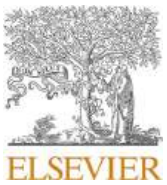

Contents lists available at ScienceDirect

Environment International

journal homepage: www.elsevier.com/locate/envint

Full length article

Modelling the anthropogenic Hg pollution fingerprint on the marine fishery production worldwide: A preliminary exposure assessment for people living in countries having different income levels

Francesco De Simone, Ian M. Hedgecock, Delia E. Bruno, Sergio Cinnirella, Francesca Sprovieri, Nicola Pirrone

CNR-Institute of Atmospheric Pollution Research, Rende 87036, Italy

ARTICLE INFO

Handling Editor: Marti Nadal

Keywords:
Mercury pollution
Mercury emissions
Mercury health hazard

ABSTRACT

Mercury is a toxic pollutant that poses risks for the human population, mainly by eating contaminated fish. Mercury is released into the atmosphere from a variety of anthropogenic activities, with levels of emissions and under policy controls that largely vary across the world, leading thus to different relative contributions to the environmental matrices. Establishing the exact sources of this contaminant in the environment is crucial to optimising the policies aimed at mitigating the exposure risks for specific populations or ecosystems. In this study, we modelled, for the first time, the fingerprint of mercury anthropogenic emissions, jointly released by source-sectors (11) and source-regions (13), on the deposition over (19) FAO fishery zones, and on the FAO official fishery productions worldwide over the 2012–2021 decade. Using mercury anthropogenic emissions for 2012 from EDGAR, East Asia and "Artisanal and Small scale Gold Mining" result the source-region and the source-sector, respectively, that contribute the most to the mercury deposition over all the FAO fishery zones. The only exception applies for the FAO fishery zone 37, the Mediterranean Sea, where the "Industrial Combustion" from the closest Europe is the pair region-sector whose joint contribution is the greatest. When normalised to the overall fishery production worldwide, representing the global fish consumption, the anthropogenic mercury fingerprint showed a similar general pattern, however with notable differences, amplifying the relative contributions of all source-sectors from East Asia and attenuating the relative contributions of the regions in the Southern Hemisphere. This fingerprint further changes when the fish consumption in countries, classified by the World Bank as having different incomes, is considered. These results demonstrate that the same anthropogenic mercury deposited on any fishery zone actually affects in a different way the different population segments worldwide. This study aims to urge the science community as well as the policy makers to use a measure that better represents the mercury hazard for human health. Further, we hope that this study, using nomenclatures that are largely used on final shelf-product, could increase the people's awareness regarding the products they consume.

1. Introduction

Mercury (Hg) is a global pollutant that poses health risks to fish-eating wildlife (Scheuhammer et al., 2007) and human populations (Sheehan et al., 2014). In its organic form, as methylmercury (MeHg), it is a potent neurotoxin (Mergler et al., 2007) that can have severe effects on cardiovascular system (Hu et al., 2021). Moreover, it can cross the placenta and affect the neurocognitive development within the womb (Axelrad et al., 2007). Most human exposure to MeHg is through fish consumption (about 60%), followed by freshwater food and rice (Zhang et al., 2010; Zhang et al., 2021). Hg ends up in ocean waters mainly via deposition processes of atmospheric Hg. Atmospheric Hg is emitted by a wide spectrum of emissions sources: natural and anthropogenic, either legacy and primary (Pirrone et al., 2010). In particular, Hg emissions from anthropogenic activities (Hg_{anthr}) are released into the atmosphere from several sectors, as estimated by a number of studies (Muntean et al., 2018; Muntean et al., 2014; Streets et al., 2019; Steenhuisen and Wilson, 2022; Munthe et al., 2019; AMAP/UNEP, 2013), each sector being characterised by a specific different mix of species and height-distribution, which have important implications for the their final fate

E-mail address: francesco.desimone@cnr.it (F. De Simone).

https://doi.org/10.1016/j.envint.2024.108891
Received 5 March 2024; Received in revised form 15 July 2024; Accepted 15 July 2024
Available online 19 July 2024

(De Simone et al., 2016).

Hg_{anthr} emissions are covered by the Minamata Convention (MC) on Mercury (www.mercuryconvention.org), a legally-binding international treaty, entered into force in 2017, aiming at world-wide reductions in human and ecosystem exposure to mercury contamination.

A recent study demonstrates mathematically that only an internationally coordinated set of abatement policies can have a significant impact on reducing Hg_{anthr} deposition worldwide (De Simone et al., 2022). However, a more detailed knowledge about the relative contribution of the different sectors of Hg_{anthr}, as emitted in different countries or regions, is critical to define and implement the most-effective abatement policies, in terms of both implementing-costs and health-benefits, especially in a transition phase, for example to mitigate the effect of Hg on a particular population segment and/or ecosystem (Bellanger et al., 2013). The link between Hg_{anthr} emissions and MeHg exposure is influenced by a complex combination of physical and chemical processes in different environmental media, regarding atmospheric emissions, transport, transformation, deposition, methylation, food chain transfer, fisheries and food consumption, all which are more or less sensitive to anthropogenic forcing and climatic variation (Zhang et al., 2021; Schartup et al., 2019; Zhang et al., 2016; Bieser et al., 2023).

A number of modelling studies have attempted to bridge the gap between Hg emission and ecosystem/health impact. The most comprehensive approach is the one of Zhang et al. (2021) where the authors evaluate the human MeHg exposure linked to Hg_{anthr} changes for a pool of future scenarios, using different coupled models (for atmosphere, soil, and ocean) and statistics from Food and Agriculture Organization (FAO, www.fao.org) and other literature sources. Other modelling studies applied simplifications, considering only some of the full set of processes highlighted above (Giang and Selin, 2016), or making use of box models (Amos et al., 2013; Angot et al., 2018). However, in all these studies, Hg, and in particular Hg_{anthr}, was considered globally, without identifying its regional or sector source.

Another class of studies employed only atmospheric models, considering the deposition as a direct measure of MeHg concentration in fishes (Giang and Selin, 2016). Some of these studies have been carried in a source-receptor framework, to tag the source of the Hg_{anthr}, either for present or future scenarios (De Simone et al., 2017; Travnikov et al., 2015; Corbitt et al., 2011). These studies have focused on individual regional or sector sources, rather than considering sources jointly in terms sectors and regions. They also generally used receptors that were not specific to the problem of Hg contaminated fish, using instead, conventional political borders or standard definitions of ocean basins.

Lavoie et al. (2018) used data of Hg concentration in fish available in a public database along with fishery statistics from FAO to estimate the Hg human exposure from global marine fisheries, however no link was established with emissions.

In this study we filled some of the gaps identified above in the literature by modelling for the first time the joint contributions of 11 source-sectors and 13 source-regions on the Hg_{anthr} deposition (i.e. the "Hg_{anthr} deposition fingerprint") on a set of 19 receptor-regions. These receptor-regions were chosen to coincide with the main FAO fishery zones (www.fao.org/fishery/en/home), for which a number of different fishery statistics are regularly released by FAO. We further used these statistics to demonstrate the power of a such source-receptor framework to obtain a preliminary Hg_{anthr} fingerprint, in terms of source-sectors and source-regions, on the fishery production in the last decade.

2. Methods

The fate of Hg was modelled using the global Hg Chemical Transport Model ECHMERIT, based on the fifth generation General Circulation Model ECHAM5 (Roeckner et al., 2003), with T42 horizontal resolution (roughly $2.8^\circ \times 2.8^\circ$at the equator) and 19 vertical levels up to 10 hPa. See Jung et al. (2009) and De Simone et al. (2014) for the technical details of the model.

2.1. Reference Hg_{anthr} emission inventory

The Emission Database for Global Atmospheric Research, at the updated version tox2 (EDGARv4.tox2, here simply referred as EDGARv4.2) (Muntean et al., 2018), was chosen as the reference inventory for the inclusion of the Hg_{anthr} emissions in the model due to its detailed features regarding the emission sectors. Indeed, the core analysis of this study is possible only by the inclusion in the model of a very detailed Hg_{anthr} emission inventory, that only the Emission Database for Global Atmospheric Research provides. This inventory provides gridded Hg global emissions from 1970 to 2012. EDGARv4.2 includes total and speciated Hg_{anthr} emissions from all key Hg source sectors:

- artisanal and small-scale gold mining (*ASGM*)
- industrial gold production (*Gold*)
- chlor-alkali production (*Chlor*)
- power generation combustion in industry (*Comb_ind*)
- residential combustion (*Comb_res*)
- cement production (*Cement*)
- glass production (*Glass*)
- non-ferrous industries (*Nfe*)
- iron and steel industries (*Iron*)
- waste incineration (*Waste*)
- road transport *Road*

The details of the Hg_{anthr} emissions for the 2012, including the speciation and geographical distribution for each sector, are reported in the Table A.2. All other technical details of this inventory can be found in Muntean et al. (2018).

This inventory, directly available in NetCDF, was interpolated to the model resolution using the second order mass conservative algorithm of the Climate Data Operators (CDO) (https://code.zmaw.de/projects/cdo). The EDGARv4.2 inventory has no information regarding the height of the Hg_{anthr} emissions. Therefore emissions were mapped to the model vertical levels by the sector characteristics, following the procedure previously described in De Simone et al. (2016).

2.2. Simulations performed

For this study three groups of simulations were performed, $Full\_Src$, $OnlyAnthr\_Src_{Rg} - Rcp$ and $OnlyAnthr\_Src_{Rg \times Sx} - Rcp$.

1) *Full_Src* ***simulations*** This first set of simulations, was performed including Hg emissions from all sources. In addition to Hg_{anthr} emissions prepared and included as described above, Hg exchange at the atmosphere–ocean interface was calculated in-line in the model, as described in De Simone et al. (2014). Monthly biomass burning Hg emissions were included off-line from GFED4s Van Der Werf et al. (2017) as described in De Simone et al. (2017). In these simulations, the prompt re-emission of freshly deposited Hg was also considered Selin et al. (2008).In this set of simulations no sources, natural, legacy or anthropogenic, were tagged. These simulations have control purposes, by the comparison against measurements. Further they provide an overall and quick idea of the ratio of primary Hg_{anthr} emissions to all other sources. See De Simone et al. (2014) for a quantitative impact of the different emissions sources on the modelled global atmospheric cycle of Hg, and De Simone et al. (2015) for the details regarding Hg emissions from Biomass Burning.

2) $OnlyAnthr\_Src_{Rg} - Rcp$ ***simulations*** This second set of simulations, was executed in a $Source_{Region} - Receptor$ framework, including only Hg_{anthr} emissions. The emission inventory was masked, at its native resolution to 13 source regions following the definition of the HTAPv2 (www.htap.org) initiative (see Fig. 1(a)) using the large area fraction algorithm included in CDO. The tagged Hg_{anthr} emissions, were then followed in the model until their deposition in one of 19 receptor regions, consisting of the ocean FAO fishery zones, illustrated in Fig. 1(b). Since we are interested in the primary impact of the Hg_{anthr} emissions,

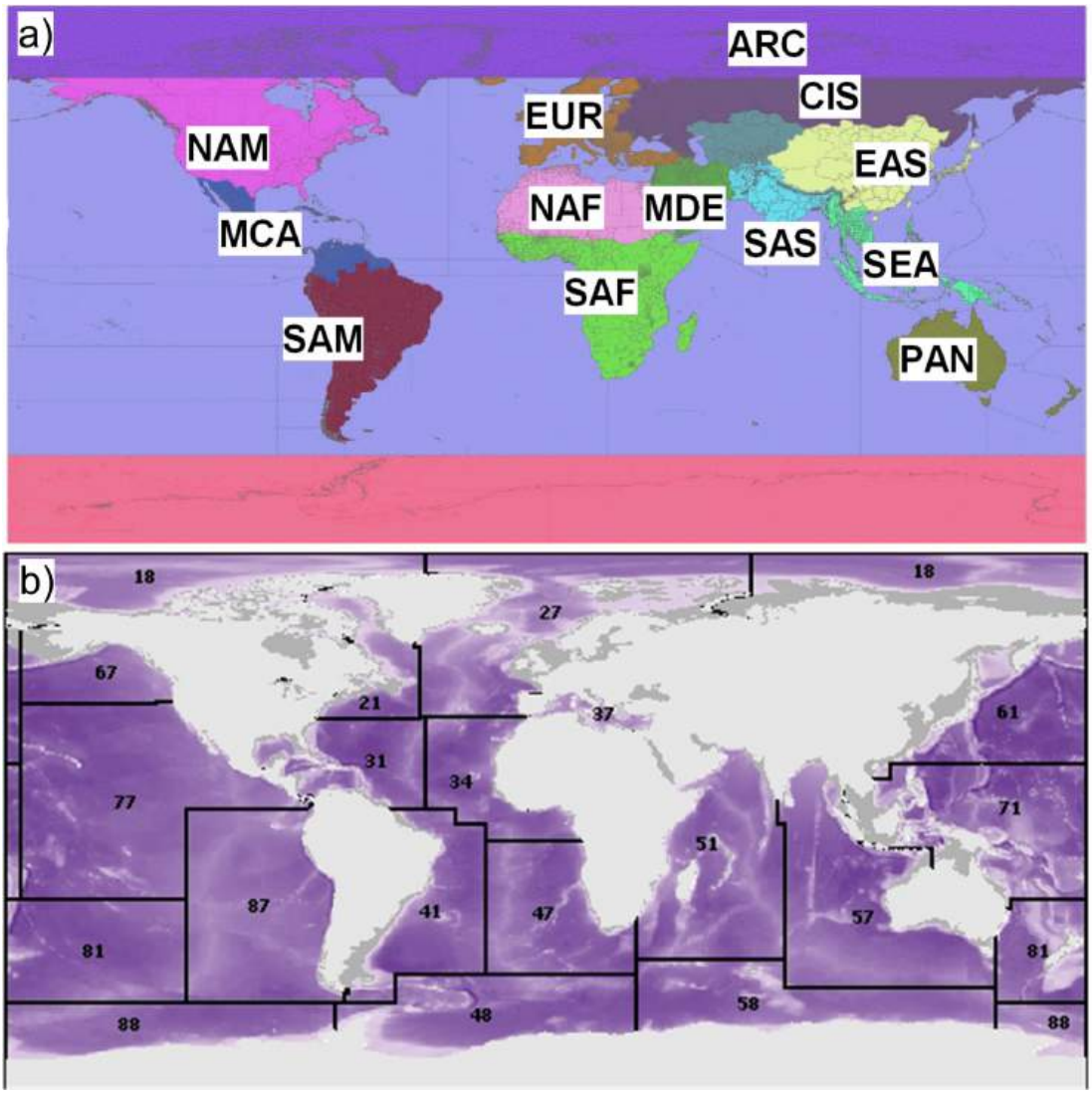

Fig. 1. Source (a) and receptor (b) regions used in this study. Legend: (a) NAM (US and Canada), EUR (Europe and Turkey), SAS (South Asia), EAS (East Asia), SEA (South East Asia), PAN (Australia and New Zealand), NAF (Northern Africa), SAF (Sub Saharan Africa), MDE (Middle East), MCA (Middle and Central America), SAM (South America), CIS (Russia and Central Asia), ARC (Arctic Circle above 66 N), and ANT (Antarctic below 60 S); (b) 18 (Arctic Sea), 21 (Atlantic, Northwest), 27 (Atlantic, Northeast), 31 (Atlantic, Western Central), 34 (Atlantic, Eastern Central), 37 (Mediterranean and Black Sea), 41 (Atlantic, Southwest), 47 (Atlantic, Southeast), 48 (Atlantic, Antarctic), 51 (Indian Ocean, Western), 57 (Indian Ocean, Eastern), 58 (Indian Ocean, Antarctic), 61 (Pacific, Northwest), 67 (Pacific, Northeast), 71 (Pacific, Western Central), 77 (Pacific, Eastern Central), 81 (Pacific, Southwest), 87 (Pacific, Southeast), 88 (Pacific, Antarctic).

for this set *OnlyAnthr_Src*$_{Rg}$ *−Rcp*, the prompt re-emission of freshly deposited Hg_{anthr} was de-activated.

3) *OnlyAnthr_Src*$_{Rg\times Sx}$ *−Rcp* ***simulations*** The third set of simulations represents the core analysis of this study. In this set, the model was run in a *Source*$_{Region\times Sector}$ *−Receptor* framework, following the Hg_{anthr} emissions from source sectors in each region to the FAO fishery zones. The direct implementation within the model of this framework would have required tagging $13 \times 11(\times 3)$ different Hg species (Hg^0,Hg^{II} and Hg^p, for each of the 11 source sectors from 13 source regions), which would have required an inordinate amount of CPU time. Therefore the *OnlyAnthr_Src*$_{Rg\times Sx}$ *−Rcp* simulation set actually consists of 11 different model runs in the *Source*$_{Region}$ *−Receptor* framework, one for each different sector of EDGARv4.2.

All the simulations were performed with a four year spin-up period to allow the atmosphere to reach steady state, then, the results from the fifth year, 2012 (or 2015 or 1998, see Section 2.3 below) were used for the purposes of the study, regardless of the reference year of the inventory employed.

2.3. Modelling the uncertainty

As there remains some uncertainty in a number of the aspects of the Hg atmospheric cycle (see, for example Ariya et al. (2015); Hynes et al. (2009); Kwon and Selin (2016); Zhou et al. (2021); Gustin et al. (2015); Horowitz et al. (2017); Bai et al. (2023)), a series of different runs was performed for the *Full_Src* and *OnlyAnthr_Src*$_{Rg}$ *−Rcp* sets of simulations to produce an ensemble taking into account a range of the variables which have a major influence, especially in connection with the Hg_{anthr} emissions and the resulting deposition (De Simone et al., 2017; De Simone et al., 2016; Travnikov et al., 2017). As analysed in details in De Simone et al. (2016), the uncertainty sources that impact the most on the resulting deposition patterns are, in order, the speciation of Hg_{anthr} emissions, the oxidation mechanism included in the model, the Hg_{anthr} emission inventory used and the height distribution of Hg_{anthr} emissions.

A first group of simulations within the ensemble were done face the uncertainty associated to the Hg_{anthr} emissions, covered by including other available inventories. Apart from the EDGARv4.2 inventory already mentioned above, and used for the core analysis of this study,

three other inventories has been included in the model in order to give a precise context in which it is possible to better analyse the results: EDGARv4.1 (estimating $1287 Mgy^{-1}$ for the year 2008, the last available (Muntean et al., 2014)), AMAP/UNEP-2010 (estimating $1960 Mgy^{-1}$ for year 2010 (AMAP/UNEP, 2013)) and AMAP/UNEP-2015 (estimating $2220 Mgy^{-1}$ for year 2015 (Steenhuisen and Wilson, 2022; Munthe et al., 2019)) using their standard speciation and height distribution. As evident, EDGARv4.1 Hg_{anthr} emission inventory estimates are quite lower than other inventories used. However, since the high uncertainties in the estimates, evaluated using a variety of methods, these emissions are well above the lower limit as assessed by AMAP/UNEP-2015 (see, for example the details of the methods (i) and (ii) in the Section "3.2.3 Uncertainties" of Munthe et al. (2019)), and therefore a good ensemble member to represent the Hg_{anthr} emissions at the lower range of the available estimates.

Regarding the height distribution, AMAP/UNEP-2010 and AMAP/UNEP-2015 were included in the model following their native distribution on three levels. Instead EDGARv4.1 inventory was processed as described for EDGARv4.2.

Four further runs were performed to specifically cover the uncertainty associated with Hg_{anthr} emission speciation and height distribution, all using the EDGARv4.2 inventory.

The remaining runs cover uncertainty associated with the atmospheric Hg^0 oxidation mechanism, the processes that can shorten lifetime of Hg^0, and the meteorological year. In particular, two chemical mechanisms were used, one based on O_3/OH oxidation scheme and one driven by Bromine, as described in De Simone et al. (2016). The meteorological years were chosen based on the nominal years of the two most recent inventories (2012 and 2015) and on the differences regarding the general circulation patters (1998), as determined by the values assumed by the major climatic indexes, like Southern Oscillation Index (SOI) (https://www.ncei.noaa.gov/access/monitoring/enso/soi) and North Atlantic Oscillation (NAO) (https://www.ncei.noaa.gov/access/monitoring/nao/), and confirmed by previous model runs (De Simone et al., 2017).

These ensembles of simulations for the *Full_Src* and $OnlyAnthr\_Src_{Rg} - Rcp$ sets were used as input to a statistical model based on bootstrapping (Mudelsee, 2014; Mudelsee, 2019), to obtain robust statistics (i.e. the mean of the ensemble) and the relative confidence intervals (CI, at the 95% level), similarly to our previous work (De Simone et al., 2017; De Simone et al., 2020; De Simone et al., 2021).

As mentioned earlier the $OnlyAnthr\_Src_{Rg\times Sx} - Rcp$ simulation set includes only the BASE runs due to computational time constraints as 13×11 simulations would have been needed to evaluate the uncertainty. Further, the AMAP emissions inventories provide less detailed information on emission sectors. Therefore for this set of model runs no explicit quantitative assessment of the uncertainty was made, although some qualitative considerations can be inferred from the results of the $OnlyAnthr\_Src_{Rg} - Rcp$ set.

The complete list of model runs performed for this study, is summarised in Table 1.

The results from the *Full_Src* model simulation ensemble, processed by bootstraping, were used to calculate the means (and the relative CI at 95% level of confidence) of the total deposition of the Hg emitted from all sources over all the FAO fishery zones, whereas $OnlyAnthr\_Src_{Rg} - Rcp$ was used to calculate the same quantities due to Hg_{anthr} emissions only. The latter was then used to establish the source-apportionment, in terms of source-regions, of the Hg_{anthr} deposition over each of the FAO fishery zones.

2.4. Fishery statistics

To evaluate the impact of Hg_{anthr} deposition and its fingerprint on fishery production worldwide, we used the official statistics from FAO, using the software FishStatJ v4.03.00 (FAO, 2023). We used the software with the workspace "FAO global fishery and aquaculture production statistics version 2023.1.2". This dataset includes annual series of total fishery and aquaculture production from 1950, distinguishing between different species of fish, crustaceans, molluscs, aquatic mammals, and other aquatic animals, residues and plants. Data include quantities farmed (aquaculture), caught and landed for both food and feed scopes in the different FAO fishery zones. Discards are excluded. Production is expressed in Mg live weight. The production source (nationality) is assigned according to the flag of the fishing vessel, unless operational contracts indicate otherwise. Since in this study we want to simply compare with the primary Hg_{anthr} deposited to the different aquaculture or fishery zones, we included all farmed and caught species, we overlook the effects of the Hg biomagnification within the food web (trophic levels), for the reasons discussed below in Section 3.5. To take in account any inter-annual variation of the production, due to anthropogenic, climatic or other causes, we used the annual average for the decade 2012–2021 in our analysis (see Table D.5). Fishery production over all FAO fishery zones represents the overall consumption of fishes, and therefore is a direct measure of the exposure to Hg_{anthr} pollution of human population worldwide.

FAO statistics are made available for single countries, or set of countries, for example grouped by income levels, according to the World Bank classification (2023 revision, datahelpdesk.worldbank.org/knowledgebase/articles/906519-world-bank-country-and-lending-groups). In this case when FAO fishery production is considered for a group of countries (see Table D.6), it doesn't necessary correspond to the fish consumption in that group, being only one component of an equation that include also import/export quota.

For the import/export quota, we used the FAO dataset "Global aquatic trade - By partner country. 2019–2021, Updated 2023". This

Table 1
Model simulations performed in this study.

	Description	*Full_Src*	$OnlyAnthr\_Src_{Rg} - Rcp$	$OnlyAnthr\_Src_{Rg\times Sx} - Rcp$
	BASE	y	y	y (11)*
Uncertainty source	Alternative			
Inventory	EDGARv4.1	y	y	n
	AMAP-2010	y	y	n
	AMAP-2015	y	y	n
Height	uniform PBL	y	y	n
	1st level	y	y	n
Speciation	Hg^0	y	y	n
	Hg^2	y	y	n
Meteo	1998	y	y	n
	2015	y	y	n
Chemistry	Br	y	y	n
	Hg^0-Short-LT	y	y	n

* This simulation actually consists of 11 different sub-runs in the $S_R - R$ framework, one for each of the 11 different industrial sectors in EDGARv2 inventory.

dataset collects the detailed statistics on world annual international trade of fishery and aquaculture products among partner countries, for the period 2019 −2021. Since the data for years 2012–2018 is not available, we used the average over the years 2019–2021 as a proxy for the whole period 2012–2021. The summary of the trade data among countries belonging to the different income levels is reported in Table D.8.

Contrarily to the Production dataset, the trade data has not indications regarding the FAO zone origin of the fish product traded. Therefore, in an first attempt to have an estimate of the Hg_{anthr} fingerprint on the fish consumption, otherwise impossible to make, for each set of countries we assumed that the distribution, in terms of FAO zone origin, of the exported fishes follows the distribution of the production, using therefore the latter as a proxy for the export distribution, as reported in the Table D.7.

2.4.1. Hg_{anthr} Fingerprints on deposition, fishery production and fish consumption

The results from the $OnlyAnthr\_Src_{Rg\times Sx}-Rcp$ set of runs were used to calculate the Hg_{anthr} fingerprint on the deposition, i.e. the relative contributions of the different source-sectors and source-regions on the resulting total Hg_{anthr} deposition over each and all FAO fishery zones.

If $Hg_{anthr}DEP^{f}_{r,s}$ is the Hg_{anthr} deposition due to a source-sector s and a source-region r over a FAO fishery zone f, the Hg_{anthr} fingerprint on the deposition over the single FAO fishery zone f can be calculated as:

$$Hg_{anthr}DEP\_Fin^{f}_{r,s} = \frac{Hg_{anthr}DEP^{f}_{r,s}}{\sum_{r,s} Hg_{anthr}DEP^{f}_{r,s}} \tag{1}$$

where $\sum_{r,s} Hg_{anthr}DEP^{f}_{r,s}$ represents the total Hg_{anthr} deposition due to all source-sectors s and source-regions r over the FAO fishery zone f.

Similarly, the Hg_{anthr} fingerprint on the deposition over all FAO fishery zones can be written as

$$Hg_{anthr}DEP\_Fin_{r,s} = \frac{\sum_{f} Hg_{anthr}DEP^{f}_{r,s}}{\sum_{r,s}\left[\sum_{f} Hg_{anthr}DEP^{f}_{r,s}\right]} \tag{2}$$

where $\sum_{f} Hg_{anthr}DEP^{f}_{r,s}$ is the Hg_{anthr} deposition due to a source-sector s and a source-region r over all FAO fishery zones, and $\sum_{r,s}\left[\sum_{f} Hg_{anthr}DEP^{f}_{r,s}\right]$ now represents the total Hg_{anthr} deposition due to all source-sectors s and source-regions r over all FAO fishery zones.

In this study the Hg_{anthr} fingerprint is further evaluated on different statistics that can be determined from FAO database, like fishery production. In this case the Hg_{anthr} deposition due to a source-sector s and a source-region r over a FAO fishery zone f is simply multiplied for a weight W^{f} that depends on the specific FAO fishery zone f, and calculated as

$$W^{f} = \frac{PROD^{f}}{\sum_{f} PROD^{f}} \tag{3}$$

where $PROD^{f}$ represents the FAO fishery production associated with the FAO fishery zone f being investigated.

Therefore, the Hg_{anthr} fingerprint on the FAO fishery production, calculated over all FAO fishery zones, can be simply written as

$$Hg_{anthr}PROD\_Fin_{r,s} = \frac{\sum_{f} Hg_{anthr}DEP^{f}_{r,s} * W^{f}}{\sum_{r,s}\left[\sum_{f} Hg_{anthr}DEP^{f}_{r,s} * W^{f}\right]} \tag{4}$$

Since the FAO statistics are also available for different countries, or set of countries, as grouped by income levels, it is further possible to evaluate the Hg_{anthr} fingerprint on the production associated with that group of countries, multiplying the Hg_{anthr} deposition due to a source-sector s and a source-region r over a FAO fishery zone f for a weight W^{f}_{i} that depends on the specific FAO fishery zone f, for that specific group i

$$W^{f}_{i} = \frac{PROD^{f}_{i}}{\sum_{f} PROD^{f}_{i}} \tag{5}$$

where $PROD^{f}_{i}$ represents the FAO fishery production of the group of countries i associated with the FAO fishery zone f.

In this specific instance, the Hg_{anthr} fingerprint on the fishery production of a specific set of countries i, calculated over all FAO fishery zones, can be simply written as

$$Hg_{anthr}PROD\_Fin^{i}_{r,s} = \frac{\sum_{f} Hg_{anthr}DEP^{f}_{r,s} * W^{f}_{i}}{\sum_{r,s}\left[\sum_{f} Hg_{anthr}DEP^{f}_{r,s} * W^{f}_{i}\right]} \tag{6}$$

where $i \in Income = \{Low, Lower-middle, Upper-middle, High\}$.

Another key FAO statistic, on which the Hg_{anthr} fingerprint can be calculated, is the consumption in a group of countries i of fishes coming from the FAO fishery zone f, defined as:

$$CONS^{f}_{i} = PROD^{f}_{i} - EXPORT^{f}_{i} + \sum_{j\neq i} IMPORT^{f}_{j} \tag{7}$$

where $EXPORT^{f}_{i}$ represents the export quota from country group i of fishes coming from FAO fishery zone f, and $IMPORT^{f}_{j}$ is the import quota from the country group j into the country group i, with $i, j \in Income$ and $j \neq i$, of the fishes coming from FAO fishery zone f.

In this instance, defining the weights W^{f}_{i} as

$$W^{f}_{i} = \frac{CONS^{f}_{i}}{\sum_{f} CONS^{f}_{i}} \tag{8}$$

the Hg_{anthr} fingerprint on the fish consumption in a specific set of countries i, calculated over all FAO fishery zones, can be simply written as

$$Hg_{anthr}CONS\_Fin^{i}_{r,s} = \frac{\sum_{f} Hg_{anthr}DEP^{f}_{r,s} * W^{f}_{i}}{\sum_{r,s}\left[\sum_{f} Hg_{anthr}DEP^{f}_{r,s} * W^{f}_{i}\right]} \tag{9}$$

where $i \in Income = \{Low, Lower-middle, Upper-middle, High\}$.

The detailed calculations of the fish consumption by FAO zone origins for the the High-, Upper-middle-, Lower-middle- and Low-income countries are reported in the Table D.9 to D.12, respectively.

2.5. Model validation

The model has been extensively tested and validated against measurements from different networks and other models over the last ten years (Travnikov et al., 2017; Angot et al., 2016; De Simone et al., 2014; De Simone et al., 2015; De Simone et al., 2016; De Simone et al., 2017), using data from different networks, including the Global Mercury Observation System (GMOS (Sprovieri et al., 2016; Sprovieri et al., 2017)) and Global Observation System for Mercury $GOS^{4}M$ ((Pirrone et al., 2022) www.gos4m.org/). Results from the comparison are presented in the Fig. C.10, and are in line with the previous studies and other models (Travnikov et al., 2017).

Given the scope of the study, we have further tested the suggested hypothesis of the proportionality between Hg concentrations in fish and

the Hg atmospheric deposition (Mason et al., 2012; SSunderland and Masonunderland and Mason, 2007; Chen et al., 2012), using available data from the literature. To this end, we have compared the Hg concentrations in sharks, an apex predator with a mean trophic level of 4, as sampled in the different FAO fishery zones, against the Hg deposition over the same FAO zones as calculated in this study (*Full* set). Data of Hg concentrations in sharks were obtained from the review of Amezcua et al. (2022), as presented in "Table 3: Estimated hazard quotients for Hg (HQ_{Hg}) in muscle of all shark species according to FAO region". The hazard quotients, reported in the table have been converted into the corresponding concentrations using the information provided in section "Human Health Risk Assessment". Shark data from the Mediterranean sea (FAO 37) were not used because of the particular conditions in the Mediterranean that enhance biomagnification, resulting in the so called "Mediterranean Hg anomaly" (Cossa and Coquery, 2005; Tesán-Onrubia et al., 2023). Shark data from the South-East Pacific (FAO 87) were also excluded due to the very few samples (3) available. The results from our comparison are reported in C.

3. Results and Discussion

The complete results from *Full_Src* and *OnlyAnthr_Src*$_{Rg}$ *−Rcp* ensembles of simulations are summarised in the Tables B.3 and B.4 within the B. The contributions to Hg deposition of all sources (natural + antropogenic) and of Hg_{anthr} emissions from each source region are reported. All the contributions represent the means of the relevant ensemble and include the relative confidence intervals (at 95% CI).

The details of the results in the Tables B.3 and B.4 are described below.

3.1. How Hg_{anthr} primary emissions contribute to deposition

The ratio between the deposition due to Hg_{anthr} primary emissions and the Hg deposition from all sources over the different FAO fishery zones has been calculated, and is presented, as a percentage in Fig. 2.

It appears evident that the relative contribution of Hg_{anthr} emissions on the deposition is a minority, and that the natural and legacy Hg emissions source contribute the most. However, this study will focus on primary Hg_{anthr} emissions for general public awareness and policy purposes. Indeed, only primary Hg_{anthr} emissions are directly and readily affected by any abatement policy.

The relative contribution of Hg_{anthr} from all source-regions ranges from a minimum of ≈ 10%, for the most remote FAO fishery zones of the southern hemisphere (FAO 48, 58 and 88), to just over 20%, for FAO 18, the Arctic Sea. However, due to the large uncertainty, the contributions of Hg_{anthr} emissions on the Hg deposition over the different FAO Fishery zones are statistically indistinguishable (at 95% level of confidence), although differences arise when considering the impacts of the individual source-regions.

In this regard, Fig. 3 indicates the origins, in terms of major source-regions, of the primary Hg_{anthr} deposited over the different FAO fishery zones.

East Asia (EAS) is the major contributor to all the FAO fishery zones. For this reason, the Fig. 3 reports the other region(s) which also contribute significantly (at 95% level of confidence) to Hg_{anthr} deposition for each FAO fishery zone. The only exception is FAO 37 (Mediterranean Sea), where the EAS contribution is statistically indistinguishable from that of EUR, and the predominantly southern hemisphere fishery zones (87, 81, 88, 57, 48, 41, 47, 58, and 51) where the EAS contribution is statistically indistinguishable from those of SAF and/or SAM.

Regarding the particular situation of FAO 37, among other driving

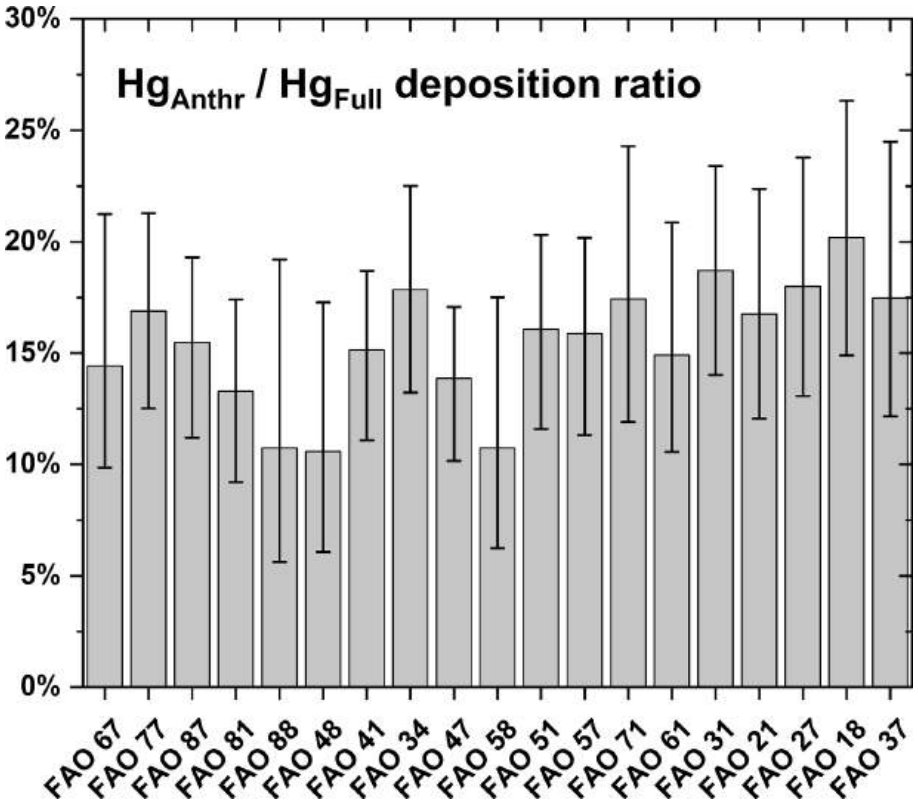

Fig. 2. Ratio of Hg_{anthr} to Hg (from all source) deposition over the different FAO fishery zones. Bars represents the ratio between the means from the *OnlyAnthr_Src*$_{Rg}$ *−Rcp* and *Full_Src* ensembles. CIs at 95% level of confidence are also reported.

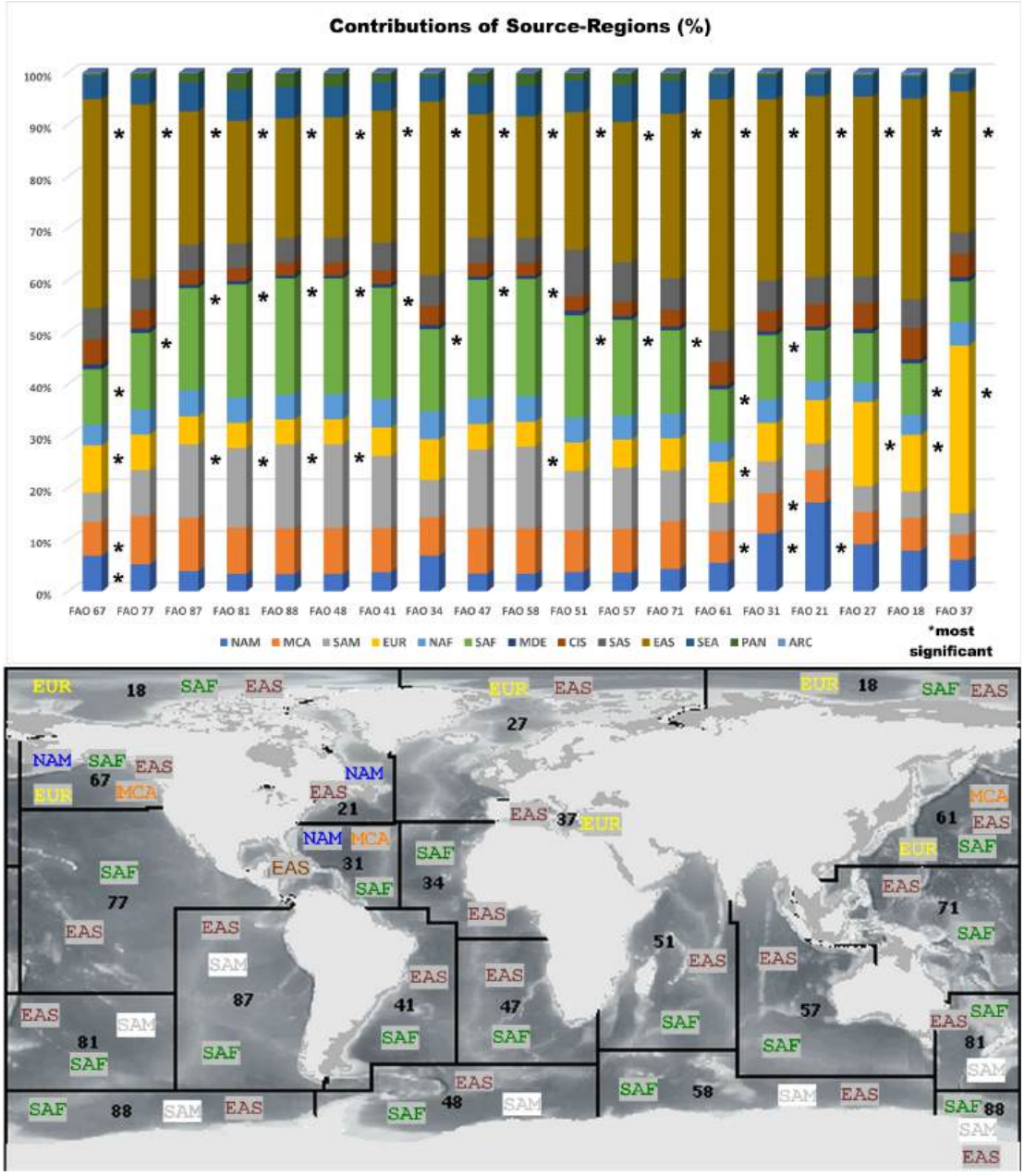

Fig. 3. Upper Panel: Contribution, in %, of the S_R to the primary Hg_{anthr} deposited over the different FAO fishery zones. Label (*) indicate EAS, that is the major, and the remaining region(s) contributing the most to the Hg_{anthr} deposition (at 95% level of confidence). Lower Panel: Geographical distribution of the major contributors.

factors, it is likely to depend on the general circulation pathways that converge over the Mediterranean area, as well known in the literature (Lelieveld et al., 2002; Gencarelli et al., 2014). Indeed, apart from the two major indistinguishable contributors (EAS and EUR), there are 8 source-regions which contributions are indistinguishable at the third place: NAM, MCA, SAM, NAF, SAF, CIS, SAS and SEA (see Fig. E.31), a situation quite similar to previous findings reported in De Simone et al. (2017). Due to the different sets of receptors used in other similar previous source-receptor studies, a detailed comparison for other FAO zones is quite difficult.

However, generally, the source-regions that contribute the most to the Hg_{anthr} deposition in the different FAO fishery zones follow the distribution of the Hg_{anthr} emissions combined with atmospheric general circulation patterns. Apart from EAS, the major emitter which contributes significantly everywhere, EUR and NAM, whose Hg_{anthr} emissions consist of a mix of Hg^0, Hg^2 and Hg^p, mostly contribute to FAO zones at near and/or medium range in the North Hemisphere. Contrarily, Hg_{anthr} emissions from SAF, consisting essentially of Hg^0 from ASGM, reaches

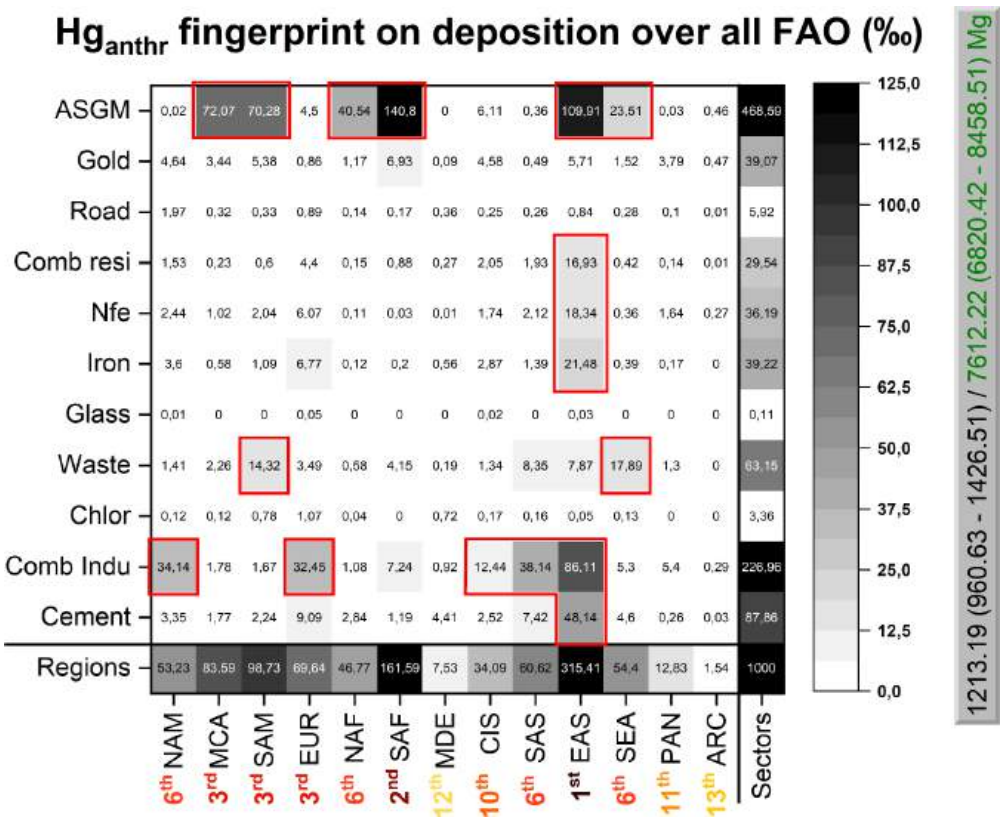

Fig. 4. Heatmap illustrating the relative joint contributions (in ‰) of source-sectors, on rows, and source-regions, on columns, on the resulting deposition of Hg_{anthr}, over all the FAO fishery zones. The last row summarises the total contributions of the source-regions, whereas the last column summarises the total contributions of the source-sectors. Red overlying areas highlight the combinations of source-sectors and source-regions whose contribution is above the chosen threshold of 1%. The side box reports, in Mg/y the total deposition due to Hg_{anthr} primary emissions respect to the Hg deposition from all sources, with the relative C.I. (at 95% level of confidence). The bottom score illustrates the rank of the regions regarding their contribution to Hg_{anthr} deposition. Shared ranks indicate regions whose contributions are statistically indistinguishable (at 95% level of confidence).

the global pool and therefore contributes significantly to a large number of FAO zones even at high northerly latitudes. The SAM contribution is more limited to the FAO zones in the Southern Hemisphere.

3.2. Hg_{anthr} fingerprint on the deposition

Results from the $OnlyAnthr\_Src_{Rg\times Sx} - Rcp$ simulation, illustrating the Hg_{anthr} fingerprint on deposition over the FAO fishery zones, are presented by means of heatmaps depicting the relative joint contributions (in ‰) of source-sectors (rows), and source-regions (columns), Fig. 4.

In order to make the heatmaps more legible, we choose to compare the contributions of the different source-sectors and source-regions relative to a threshold of 1% (i.e. 10 ‰).

A pattern is clearly evident in the figure, that partially resembles the observations done independently for source-regions apportionment, but enables a more detailed description of the fate of Hg_{anthr} emissions, confirming the hypotheses made during the analysis of the previous section.

The rows of *ASGM*, *Comb_indu*, *Cement* and *Waste*, 470, 227, 88 and 63 ‰respectively, markedly dominate over all other sectors. However, if the Hg_{anthr} from *ASGM* originates essentially from regions of the southern hemisphere (SAM, SAF), tropics, (MCA, NAF), and Asia (EAS and SEA), the Hg_{anthr} emitted by *Comb_indu* originates in the most industrialised countries (NAM, EUR, CIS, EAS and SAS). The contribution from *Cement* is largely from EAS, whereas for *Waste*, the Hg_{anthr} from this sector mainly comes from SAM and SEA. The contribution of *Chlor*, *Glass*, *Road* and *Gold*, is everywhere below the threshold of 1%.

EAS is the major contributor (315 ‰) to Hg_{anthr} deposition over FAO fishery zones, with contributions from a number of individual source sectors well above the 1%. SAF follows as the second most important (162 ‰) with Hg_{anthr} emissions essentially all from *ASGM*.

Regarding the Hg_{anthr} source sector fingerprints on the deposition over each FAO fishery zone (Figs. E.12 to E.30 in E), *ASGM* is most important contributor, accounting for more than 50% in FAO 87, 81, 88, 48, 41, 47 and 58. The Mediterranean (FAO 37) is the only exception, where *Comb_indu* contributes $3.7Mg(34\%)$ annually, versus the $3.4Mg(31\%)$ from *ASGM*.

3.3. Hg_{anthr} fingerprint on fishery production

As explained in the introduction, the redefinition of the receptor areas to match the FAO fishery zones allowed us to conduct specific analysis integrating the official statistics available from FAO regarding the fishery production. This is particularly useful for the evaluation of the impact of the Hg pollution, since human exposure mainly occurs by consumption of contaminated fish, and the fishery production over all of

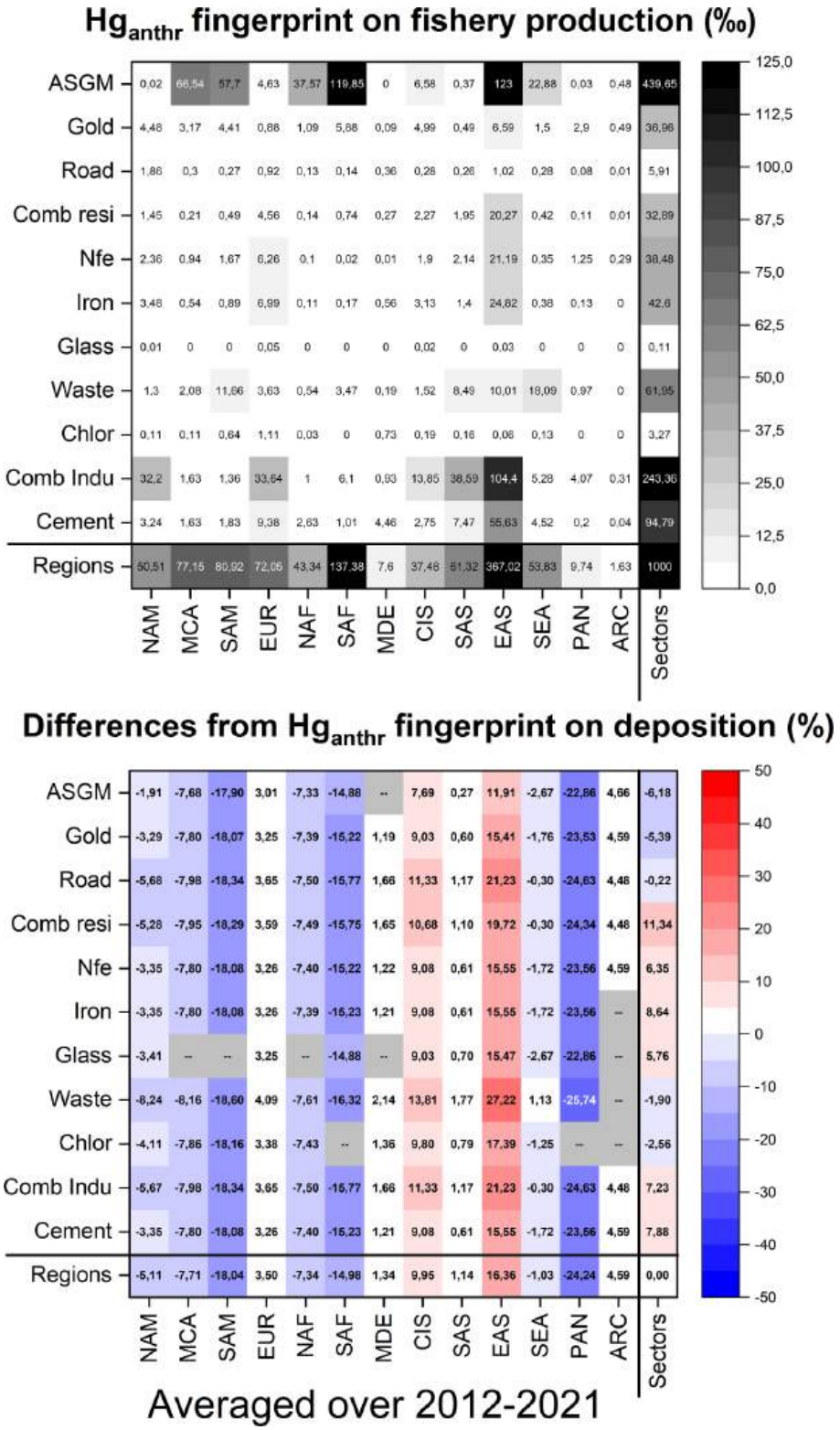

Fig. 5. In the upper panel, the heatmap illustrating the relative joint contributions (in ‰) of source-sectors, on rows, and source-regions, on columns, on the resulting deposition of Hg_{anthr}, over all the FAO fishery zones, and normalised by the fishery production in the pertinent FAO fishery zones averaged over the 2012–2021 period. The last row summarises the total contributions of the source-regions, whereas the last column summarises the total contributions of the source-sectors. In the lower panel the heatmap of the difference, in %, between the Hg_{anthr} fingerprint on the fishery production and Hg_{anthr} fingerprint on the deposition, as in Fig. 4. The last row here reports the total differences for the source-regions, whereas the last column reports the total differences for the. source-sectors.

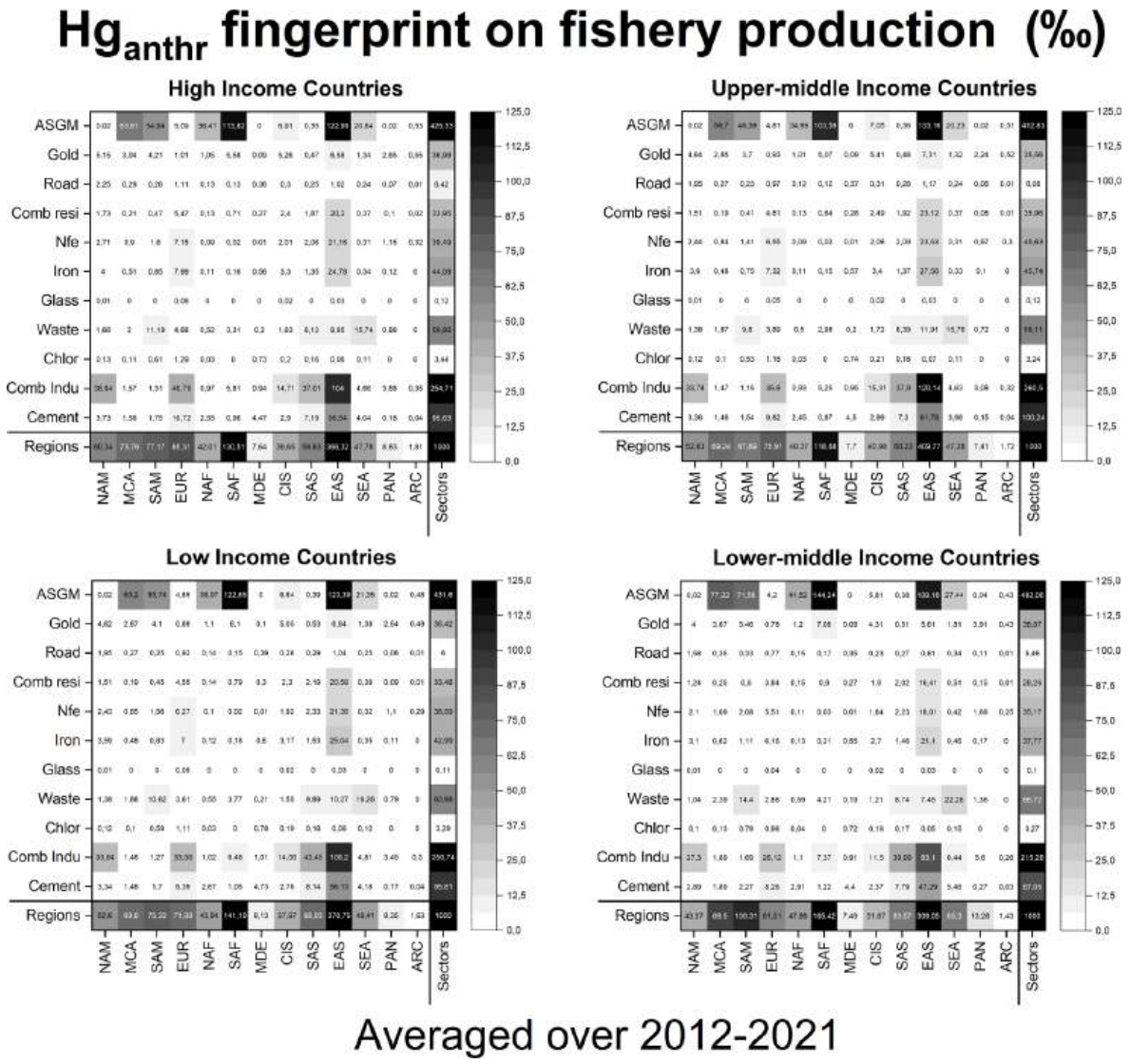

Fig. 6. Heatmap illustrating the relative joint contributions (in ‰) of source-sectors, on rows, and source-regions, on columns, on the resulting deposition of Hg_{anthr}, over all the FAO fishery zones, and normalised by the fishery production in the pertinent FAO fishery zones of countries classified by World Bank as having High, Upper-middle, Lower-middle and Low Income, respectively. Production data are averaged over the 2012–2021 period. In each heatmap, the last row here reports the total contributions for the source-regions, whereas the last column reports the total contributions for the source-sectors.

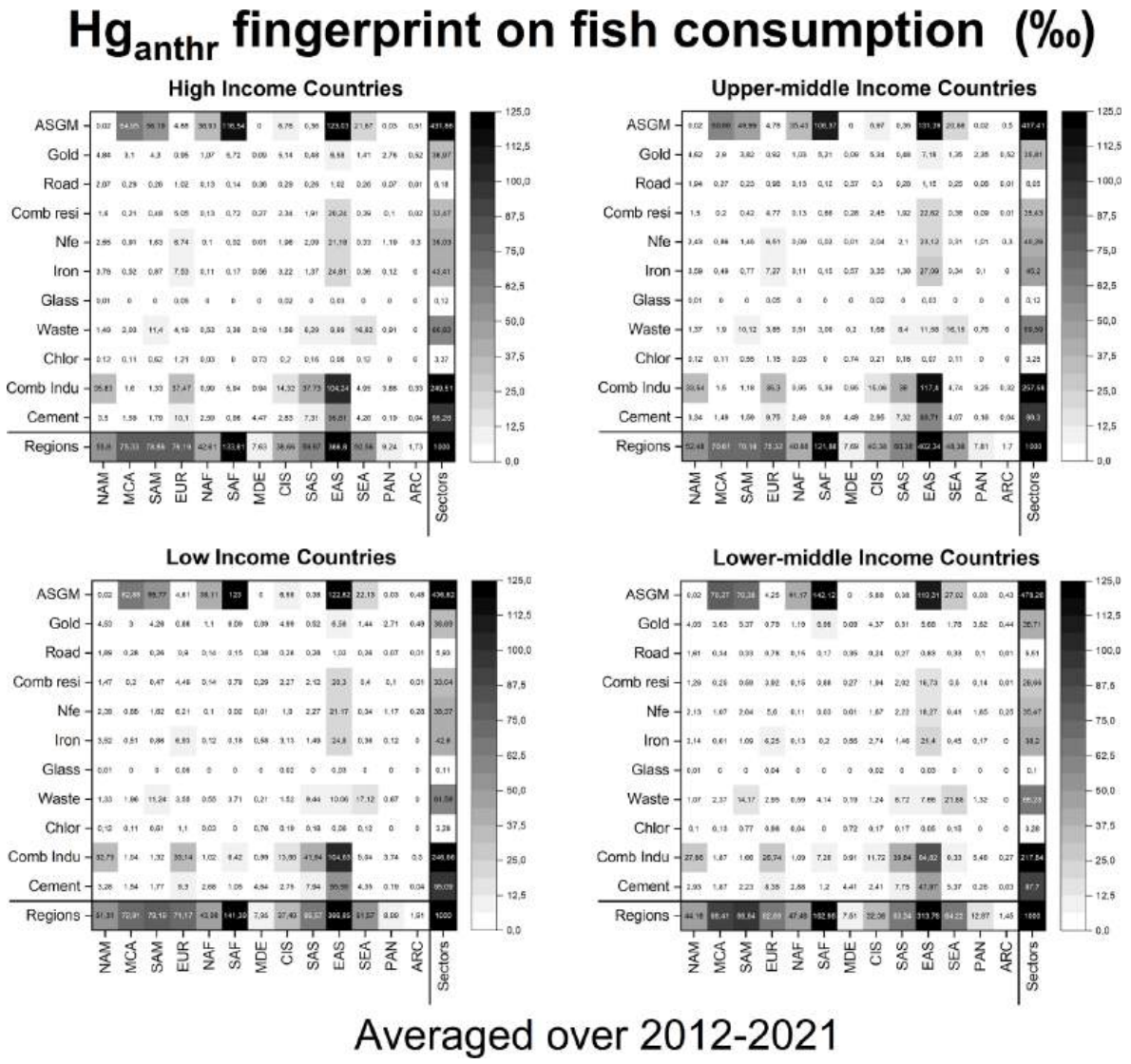

Fig. 7. Heatmap illustrating the relative joint contributions (in ‰) of source-sectors, on rows, and source-regions, on columns, on the resulting deposition of Hg_{anthr}, over all the FAO fishery zones, and normalised by the consumption of fish from the pertinent FAO fishery zones into countries classified by World Bank as having High, Upper-middle, Lower-middle and Low Income, respectively. Consumption data are averaged over the 2012–2021 period. In each heatmap, the last row here reports the total contributions for the source-regions, whereas the last column reports the total contributions for the source-sectors.

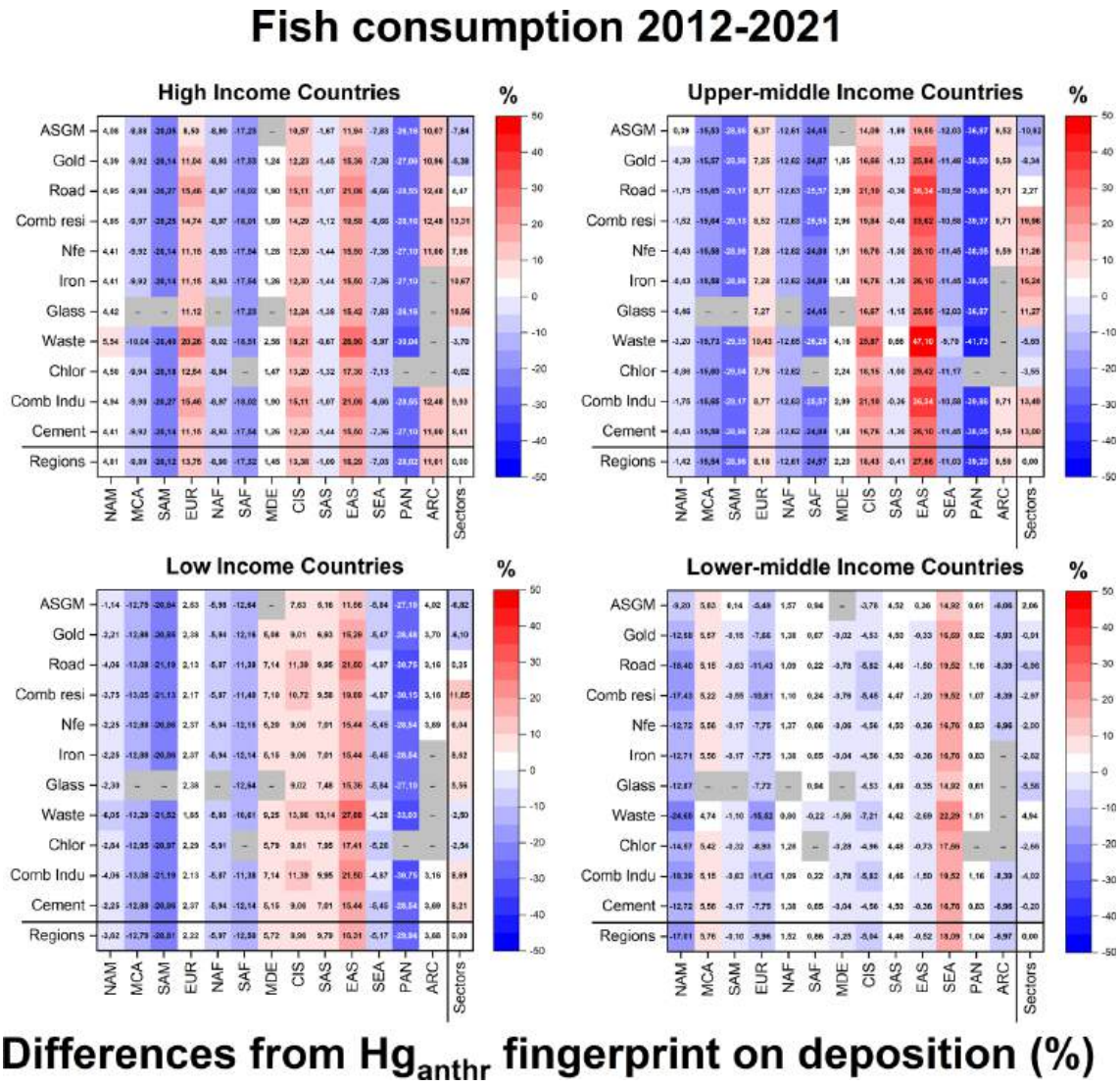

Fig. 8. Heatmaps illustrating the difference, in %, between the Hg_{anthr} fingerprint on the deposition and the Hg_{anthr} fingerprint on the fish consumption in the countries classified by World Bank as having High, Upper-middle, Lower-middle and Low Income, respectively. In each heatmap, the last row here reports the total differences for the source-regions, whereas the last column reports the total differences for the source-sectors.

the FAO fishery zones represents a direct measure of this exposure for human population worldwide.

The Hg_{anthr} fingerprint on deposition over all FAO fishery zones has been recalculated, normalising it to the fishery production in each zone, as described in Section 2.4.1. The output of this analysis is presented in the Fig. 5.

The Hg_{anthr} fingerprint on the fishery production has a pattern that is very similar to that of Hg_{anthr} deposition, with the same characteristic hot spots already mentioned for Fig. 4. However, a close look reveals some important differences. As is evident in the lower panel of the percentage differences between the two Hg_{anthr} fingerprints, the contributions of all sectors from EAS are further amplified by ≈ 12% to 27%, total 16%, when normalised by the fishery production. In particular, the *Waste* sector from EAS now exceeds our threshold of 1%. This is likely due to the fact that EAS is the region that contributes the most on the deposition over all FAO fishery zones, including those of intensive aquaculture that are particularly productive. The other source-region whose contributions are systematically amplified is CIS, with a global positive differences just below 10%. On the contrary, the regions whose contributions decreased much, SAM (-18%), SAF (≈ −15%) and PAN are entirely or mostly in the Southern Hemisphere, where FAO fishery zones are less intensively harvested. PAN in particular declines by almost a quarter (≈ −24%). The remaining regions appears to be quite neutral regarding their contributions with or without the normalisation to fish productions. This is the case in particular for EUR, SAS, SEA and ARC. Regarding source-sectors, *Comb_res* is the one whose contribution changes the most (11%)

3.4. Hg_{anthr} fingerprint on the fish consumption in countries having different incomes

The FAO statistics about the fishery harvest are provided by nationality. This information allows for further analysis, in particular to investigate the fingerprint of Hg_{anthr} emissions on the fishery production and fish consumption in countries belonging to different classifications according to the World Bank. This is crucial to have a preliminary idea on the effects the Hg_{anthr} pollution may have on the population belonging to countries having different income levels, especially the most vulnerable ones.

The first results from this analysis are reported in the four panels of the following Fig. 6, depicting the Hg_{anthr} fingerprint on the fishery production of the countries classified by the World Bank as having High, Upper-middle, Lower-middle and Low Income, respectively.

The general patterns of the Hg_{anthr} fingerprints on the fishery production of the countries belonging to different income levels is rather similar to the Hg_{anthr} fingerprint on the global fishery production reported in Fig. 5. However, important differences arise when looking at the single contributions. For example, if total contributions from *SEA* on the production of High and Low Income countries are very close to that of global production (approximately 370 ‰), the contributions of *SEA* on the production of other countries diverge, at approximately 410 ‰for Upper-middle and approximately 310 ‰for Lower-Middle Income countries. This is due to the different FAO fishery zones used by these two sets of countries, as illustrated in Table D.7 and in the Fig. D.11. Production for Upper-middle Income countries comes mostly from the FAO 61 (74%), that is the most impacted by Hg_{anthr} of the near *EAS*, whereas for Lower-middle Income countries the production from this zone is negligible. A number of other similar examples exists: the contributions of *NAM* and *EUR* to production of High Income countries rise from 50‰to 60‰and from 72‰to 85‰, respectively, due to the intensive use of the impacted FAO zones 27 (31%) and 67 (10%). Instead for Lower-middle Income countries the contribution of *SAF* rises from 140‰to 165‰due to the intensive use of FAO zones 71 (64%) 57 (16%) and 51 and 34 (both 10%) that are impacted by *SAF*.

Differently from the production calculated over all FAO fishery zones and depicted in Fig. 5, the production of a country, or in this case a set of countries, doesn't necessary represent the fish consumption in that country, or set of countries. Therefore, to have an indication of the exposure to Hg pollution of the people living therein, the production has to be corrected for the relevant import/export quota, in order to give the consumption.

Therefore, the Hg_{anthr} fingerprint on deposition over all FAO fishery zones has been recalculated for each set of countries, normalising it to the consumption of fish coming from each FAO fishery zone, as described in Section 2.4.1.

This analysis is summarised in Fig. 7, in which the four panels show the Hg_{anthr} fingerprint on the consumption in the countries classified by the World Bank as having High, Upper-middle, Lower-middle and Low Income, respectively.

As evident by the comparison with the Fig. 6, the Hg_{anthr} fingerprint on fish consumption substantially does not change from that on production, for all of the sets of countries analysed. This depends on a number of factors. For countries belonging to Upper-Middle and Lower-Middle income set, the quota of import and export is marginal and the distribution by FAO fishery zones of production and consumption is quite unaltered, see Table D.13. For Low and High income countries the situation is quite different because the import/export quota reaches about one half of the production. However, the changes in the distribution of fish consumption by FAO fishery zones are such that the impact Hg_{anthr} emissions in terms of sources remains quite unaltered. For example, for Low income countries, the weight of FAO 71 rises to 7%, whereas the weights of FAO 51 and 34 decrease roughly of the same amount (Table D.13). However, noticeably all these FAO zones are impacted the most by the same *SAF* and *EAS* (Fig. 3) regions, attenuating thus the differences.

In a similar way we done for the fishery production worldwide in the Fig. 5, we calculate the percentage differences between the Hg_{anthr} fingerprint on fish consumption in each of the different sets of countries and the Hg_{anthr} fingerprint on the raw deposition. This comparison provides an answer to the policy relevant question: "How much does the exposure to Hg_{anthr} of populations living in countries having different income levels differs when comparing calculated consumption to simple Hg_{anthr} deposition patterns?" The results of this comparison are presented in the four panels of the following Fig. 8.

When normalised to fish consumption in high income countries, the impact on the Hg_{anthr} fingerprint of most of the regions near the Arctic circle is particularly amplified, due to the fact that the FAO 27 is the most used fishery zone by these countries. The contribution of both EUR and CIS is increased by 13% over all sectors and roughly the 20% for *Waste*, whereas for ART, the contribution rise is roughly the 11%. The contribution of NAM remains quite unaltered. However, EAS is the region for which this positive amplification reaches the maximum (16%), ranging from 12% for *ASGM* to 27% for *Waste*. On the contrary, the regions for which the differences are negative, are PAN (approx. −28%), SAM (-20%) and SAF (-17%), and MCA, NAF and SEA (≈ −7 to −10% for all sectors). The contributions of the remaining regions, MDE and SAS, remain more or less unaltered. It is interesting to note that *Waste* is the sector whose contributions for single regions changed the most in the Hg_{anthr} fingerprints, in both directions, although the overall difference for this sector is roughly neutral. The sectors whose contributions

changed the most are *Comb_resi* (+13%) *Glass* and *Iron* (+11%) and *Comb_indu* and *Cement* (roughly + 10%).

For Upper-middle income countries the tendency is similar to that of High income countries. The EUR contribution is still positive but is below the 10% over all sectors, except for *Waste*. The differences of ARC on the Hg_{anthr} fingerprint remains positive at about 10% for all sectors. The differences for other regions are more accentuated. EAS region sees its overall contribution difference rise by 20%, and above 45% for *Waste*. Also the contribution difference of CIS increases by 25% for *Waste*. On the other hand, the overall contribution differences of MCA, SAF, SAM, and PAM are in the negative range: ≈ −15%, −25%, −29% and −39%, respectively. The overall contribution difference from *ASGM* decreases from ≈ −8% for high income countries to ≈ −11% for upper-middle income countries. For these countries, the sectors that exhibit the greater differences are *Comb_resi* (≈ +20%) and *iron* (above + 15%).

The situation changes noticeably for the Hg_{anthr} fingerprints on the fish consumption in Lower-Middle and Low income countries. For the first in particular the context is almost neutral. It is the only group for which EUR and ARC contribution differences decrease to ≈ −10% and −7%, respectively. The NAM contribution difference also decreases at −17% (down to −25% for *Waste*). The SEA contribution difference is the only one that increases (18%), whereas the contributions of all other regions, including EAS, remain roughly similar.

For low income countries the Hg_{anthr} fingerprint differences lie in the positive fields for the MDE, CIS, SAS and EAS regions, whereas the contribution differences for PAN, SAM SAF and MCA became strongly negative. *Comb_res* is the only sectors whose contribution differences change in an appreciable way, i.e. above + 10%.

3.5. Limitations of this work and further developments

In this study, in the normalisation by fish production, we have implicitly considered the total deposition of Hg_{anthr} over FAO fishery zones as a direct measure of the Hg marine biota, namely fish, concentrations following other similar studies and conclusions (Giang and Selin, 2016). This may seem a rather improper assumption for a number of reasons. The first is related to the complex physical and chemical processes that link the inorganic Hg deposited over an area which can be transformed to MeHg and enter the food chain (and biomagnify) or be re-emitted to the atmosphere (Bieser et al., 2023; Zhang et al., 2020). However, many of the processes driving the biomagnification of Hg in fish are external forces, often anthropogenic in nature, such as overfishing of particular species, or changes in local water temperatures that can lead the fish of the higher trophic levels to modify their preferred foraging territories and/or depths (Cheung et al., 2009; Schartup et al., 2019). Nevertheless, as suggested by a number of studies (Mason et al., 2012; SSunderland and Masonunderland and Mason, 2007; Chen et al., 2012), it seems that fish concentrations respond proportionally to atmospheric deposition over years to decades, although with local differences (Knightes et al., 2009; Selin et al., 2010; Drenner et al., 2013).

This proportionality between Hg fish concentrations in the different FAO fishery zones and the Hg atmospheric deposition over the same regions has been further tested and confirmed in this study using existing literature data for sharks, as reviewed in Amezcua et al. (2022), see Section C.

Since the lack of information regarding the FAO fishery zone origins of fishes traded in the trading sheets from the FAO database, in order to estimate the fish consumption in a given set of countries we made some assumptions. We assumed that the distribution in terms of FAO fishery zones of the exported fishes for a set of countries follows the distribution of the production for that set of countries. This is an unavoidable simplification. However, more detailed information about the traded species of fishes, if any, have to be cross-checked among different commodity-trade-specific databases (see https://wits.worldbank.org/ for an example) not readily available, and which surely require complex data manipulation (or other different simplifications) to map the fish species to the commodity codes generally used in these database. Moreover, trading sheets from FAO database report data only for the period 2019–2021, and therefore we were somewhat obliged to use the average over this time window as proxy for the entire 2012–2021 period analysed for the production. The acquisition of more detailed information and data to have a more accurate estimate of the fish consumption in the different countries deserves separate and thorough future studies.

We used EDGARv4.2 as the reference Hg_{anthr} emissions inventory for the core analysis of this study, although it is released for the nominal year 2012. It is known in the literature that the Hg_{anthr} emissions could have changed over the last decade (Wu et al., 2020; Sun et al., 2024), however the more recent inventories available, in particular Streets et al. (2019); Steenhuisen and Wilson (2022); Munthe et al. (2019), are not available with the details of EDGARv4.2, and therefore also a comparison is rather difficult. In the future, when the new version of this database becomes available, or when other inventories will be released at such level of source-sector details, we intend to release an updated analysis, integrating more detailed trade information to follow the link from Hg_{anthr} emissions to deposition to fishery to consumer in the single world countries.

4. Conclusion

Identifying the Hg_{anthr} pollution sources in detail, i.e. in terms of both sectors and regions, using the best source apportionment technique (s) available, is a critical factor in identifying the most effective emissions reduction strategies tailored for ecosystems, specific regions/fisheries or populations at risk.

In this study, we have shown, for the first time, the detailed Hg_{anthr} fingerprint on the deposition over the FAO fishery zones. Moreover, we highlighted how this critical and very useful information, especially from a policy point of view, can be best interpreted when cross-referenced with data coming from other databases. The Hg_{anthr} fingerprint on the actual FAO fishery production, corresponding the consumption of fishes worldwide, although having a general pattern similar to that of the Hg_{anthr} deposition fingerprint, shows notable differences, strongly amplifying the relative contributions of some source sectors and/or regions and attenuating the relative contributions of others, particularly those in the Southern Hemisphere. These marked differences can be re-interpreted when the fish consumption by countries, classified by World Bank as having different incomes, is considered.

This work is a important starting point for reflection about a couple of facts.

Firstly, an appropriate measure should be considered in developing a policy, and in order to evaluate or monitor the effects of the same. In

particular a suitable and direct exposure indicator should be considered for environmental problems having an impact on public health. Policy, academia and the markets should question the wisdom of sustain the current air concentrations monitoring programs with more robust measurements of Hg concentration in fishes, possibly extending the regulatory standards with the inclusion of more sophisticated experimental equipment, in order to have more insight into the depth and breadth of Hg pollution.

Secondly, but not less important from a scientific point of view is the demand for the effective development of research infrastructures that can provide researchers with tools that allow for queries to different integrated and federated databases from different certified sources. This would facilitate the efforts required to carry out similar studies that link chemical exposure and population health, as is the scope of the Environmental Exposure Assessment Research Infrastructure (EIRENE) (www.eirene-ri.eu/), for example, potentially shortening the required time from months to few clicks.

Funding sources

The Authors would acknowledge the contribution received from the European Union's Horizon Europe research and innovation programme under the EIRENE PPP project (Grant Agreement: 101079789).

Declaration of Competing Interest

The authors declare that they have no known competing financial interests or personal relationships that could have appeared to influence the work reported in this paper.

Data availability

Data will be made available on request.

Appendix A. Details of EDGARv4.2 Hg_{anthr} Emission inventory

Table A.2: Detailed emissions of EDGARv4.2

Sector	Emissions			Geographical distribution (%)												
Name	Hg^0	Hg^2	Hg^P	**NAM**	**MCA**	**SAM**	**EUR**	**NAF**	**SAF**	**MDE**	**CIS**	**SAS**	**EAS**	**SEA**	**PAN**	**ARC**
artisanal and small-scale gold mining (*ASGM*)	811.355			0.00	15.03	14.23	1.05	8.81	29.58	0.00	1.42	0.08	24.77	4.91	0.01	0.11
cement production (*Cement*)	136.275	25.552	8.517	4.00	1.84	2.26	10.95	3.08	1.25	5.11	3.01	8.63	54.79	4.78	0.26	0.04
chlor-alkali production (*Chlor*)	5.363	2.298		3.73	3.36	20.41	34.06	0.99	0.00	21.95	5.51	4.96	1.60	3.43	0.00	0.00
power generation combustion in industry (*Comb_ind*)	231.409	185.127	46.224	15.75	0.68	0.63	15.19	0.44	2.84	0.41	5.75	17.03	37.10	2.03	2.02	0.13
residential combustion (*Comb_res*)	32.388	19.880	5.124	5.45	0.70	1.74	15.91	0.46	2.70	0.92	7.27	6.69	56.45	1.26	0.41	0.05
glass production (*Glass*)	0.171	0.032	0.011	12.00	0.00	0.00	45.50	0.00	0.50	0.00	15.50	2.00	23.00	0.50	1.00	0.00
iron and steel industries (*Iron*)	62.375	11.695	3.898	9.50	1.34	2.43	18.04	0.30	0.47	1.42	7.58	3.59	54.07	0.89	0.37	0.00
industrial gold production (*Gold*)	56.563	10.774	2.693	12.95	8.38	12.74	2.42	2.98	17.07	0.24	12.80	1.33	15.21	3.71	8.86	1.31
non-ferrous industries (*Nfe*)	52.954	9.945	3.294	7.06	2.56	5.01	17.71	0.28	0.07	0.04	5.05	5.99	50.59	0.89	3.96	0.78
road transport *Road*	6.047	4.837	1.209	35.08	4.82	4.77	15.97	2.22	2.53	6.07	4.44	4.44	13.95	4.08	1.46	0.16
waste incineration (*Waste*)	25.563	76.689	25.563	2.63	3.36	20.77	6.62	0.91	6.32	0.33	2.50	14.90	13.36	26.41	1.90	0.00

Appendix B. Detailed results of *Full_Src* and *OnlyAnthr_Src*$_{Rg}$ *−Rcp* model simulations

Table B.3: Detailed results of *Full_Src* and *OnlyAnthr_Src*$_{Rg}$ *−Rcp* model simulations/Part 1

Region	67	77	87	81	88	48	41	34	47
NAM	2.24 (1.87–2.67)	11.68 (9.56–14.08)	3.43 (2.57–4.23)	1.71 (1.23–2.11)	0.15 (0.10–0.19)	0.48 (0.34–0.62)	2.02 (1.52–2.48)	4.31 (3.77–5.12)	1.64 (1.21–2.01)
MCA	2.15 (1.68–2.65)	21.20 (18.83–22.84)	9.05 (8.02–9.83)	4.55 (3.46–5.47)	0.40 (0.27–0.54)	1.30 (0.91–1.71)	4.58 (3.66–5.22)	4.63 (3.91–5.18)	4.25 (3.26–4.95)
SAM	1.83 (1.32–2.27)	19.92 (16.00–23.02)	12.42 (10.56–13.64)	7.78 (6.21–9.07)	0.73 (0.52–0.96)	2.34 (1.78–2.95)	7.52 (6.60–8.18)	4.52 (3.50–5.32)	7.30 (6.11–8.16)
EUR	2.96 (2.62–3.46)	15.59 (12.67–18.04)	4.79 (3.56–5.76)	2.49 (1.85–2.99)	0.22 (0.15–0.28)	0.70 (0.49–0.89)	2.96 (2.24–3.52)	4.85 (4.25–5.37)	2.40 (1.78–2.86)
NAF	1.32 (0.91–1.73)	10.69 (7.54–13.20)	4.39 (3.00–5.67)	2.46 (1.59–3.25)	0.22 (0.13–0.32)	0.71 (0.43–1.00)	3.03 (2.23–3.64)	3.38 (2.57–3.97)	2.45 (1.63–3.13)
SAF	3.48 (2.43–4.40)	33.34 (24.50–40.33)	17.22 (13.00–20.35)	11.05 (8.41–13.18)	1.00 (0.69–1.34)	3.22 (2.32–4.18)	11.54 (9.21–13.22)	9.87 (7.58–12.09)	10.98 (8.77–12.51)
MDE	0.28 (0.22–0.34)	1.76 (1.42–2.07)	0.58 (0.44–0.70)	0.32 (0.23–0.39)	0.03 (0.02–0.04)	0.09 (0.06–0.12)	0.38 (0.30–0.46)	0.51 (0.41–0.61)	0.31 (0.23–0.38)
CIS	1.58 (1.36–1.89)	8.16 (6.43–9.51)	2.41 (1.78–2.86)	1.26 (0.92–1.51)	0.11 (0.07–0.14)	0.35 (0.25–0.45)	1.47 (1.09–1.74)	2.34 (1.83–2.72)	1.21 (0.89–1.43)
SAS	1.97 (1.44–2.42)	13.52 (10.00–16.29)	4.36 (3.01–5.57)	2.41 (1.60–3.08)	0.21 (0.13–0.29)	0.68 (0.44–0.92)	2.81 (1.93–3.55)	3.70 (2.68–4.54)	2.38 (1.59–3.02)
EAS	13.15 (11.89–15.15)	75.81 (64.96–83.41)	22.60 (17.20–26.14)	11.99 (8.96–14.09)	1.04 (0.72–1.37)	3.37 (2.40–4.29)	13.77 (10.65–15.83)	20.90 (17.17–23.45)	11.51 (8.71–13.29)
SEA	1.40 (1.08–1.73)	11.24 (8.91–12.95)	4.86 (3.71–5.68)	3.07 (2.34–3.69)	0.27 (0.18–0.37)	0.87 (0.61–1.15)	3.00 (2.28–3.50)	2.89 (2.26–3.35)	2.84 (2.14–3.35)
PAN	0.18 (0.12–0.23)	2.09 (1.56–2.52)	1.54 (1.25–1.74)	1.60 (1.31–1.91)	0.12 (0.09–0.15)	0.37 (0.29–0.46)	0.90 (0.73–1.03)	0.46 (0.33–0.56)	0.98 (0.80–1.13)
ARC	0.07 (0.05–0.09)	0.37 (0.26–0.45)	0.11 (0.08–0.13)	0.06 (0.04–0.07)	0.01 (0.00–0.01)	0.02 (0.01–0.02)	0.07 (0.05–0.08)	0.11 (0.08–0.13)	0.05 (0.04–0.07)
Anthr	32.63 (27.00–39.04)	225.37 (182.62–258.69)	87.75 (68.18–102.30)	50.75 (38.16–60.80)	4.49 (3.09–5.99)	14.50 (10.32–18.76)	54.03 (42.48–62.46)	62.45 (50.33–72.40)	48.31 (37.15–56.30)
Full	226.21 (183.80–273.98)	1334.16 (1215.33–1459.50)	566.95 (529.97–608.35)	382.24 (349.12–414.81)	41.87 (31.20–54.96)	137.06 (108.49–169.94)	356.93 (334.00–383.01)	349.90 (321.63–380.63)	348.38 (329.64–365.63)

Table B.4: Detailed results of *Full_Src* and *OnlyAnthr_Src*$_{Rg}$ −*Rcp* model simulations/Part 2

	58	51	57	71	61	31	21	27	18	37
NAM	0.49 (0.34–0.62)	3.83 (2.89–4.68)	3.53 (2.64–4.36)	7.45 (5.59–9.27)	6.29 (5.25–7.56)	5.54 (4.49–6.86)	5.22 (4.03–6.54)	2.83 (2.44–3.41)	1.07 (0.92–1.26)	0.67 (0.58–0.79)
MCA	1.29 (0.90–1.71)	8.19 (6.49–9.38)	7.95 (6.16–9.13)	15.79 (13.34–17.82)	7.04 (5.69–8.42)	3.80 (3.13–4.71)	1.94 (1.62–2.22)	1.91 (1.57–2.18)	0.86 (0.68–1.02)	0.54 (0.45–0.63)
SAM	2.29 (1.77–2.91)	11.55 (9.42–13.21)	11.29 (8.97–12.95)	16.84 (13.19–19.79)	6.13 (4.56–7.45)	3.08 (2.36–3.69)	1.54 (1.14–1.86)	1.55 (1.14–1.86)	0.70 (0.51–0.85)	0.45 (0.33–0.54)
EUR	0.71 (0.50–0.90)	5.57 (4.28–6.62)	5.15 (3.84–6.20)	10.65 (8.17–12.84)	9.10 (8.23–10.44)	3.67 (3.02–4.20)	2.54 (2.29–2.81)	5.04 (4.07–6.40)	1.49 (1.39–1.59)	3.57 (2.65–4.80)
NAF	0.70 (0.43–1.00)	4.86 (3.52–5.98)	4.54 (3.11–5.85)	8.18 (5.75–10.27)	4.31 (3.04–5.55)	2.21 (1.65–2.64)	1.13 (0.80–1.44)	1.15 (0.83–1.42)	0.53 (0.36–0.67)	0.49 (0.33–0.74)
SAF	3.29 (2.48–4.21)	20.07 (16.17–22.93)	17.58 (13.74–20.63)	27.57 (20.36–33.44)	11.58 (8.22–14.37)	6.12 (4.63–7.49)	2.97 (2.12–3.67)	2.97 (2.09–3.64)	1.34 (0.96–1.67)	0.86 (0.63–1.06)
MDE	0.09 (0.06–0.12)	0.87 (0.72–1.02)	0.68 (0.55–0.82)	1.27 (0.99–1.54)	0.90 (0.74–1.07)	0.39 (0.31–0.47)	0.23 (0.19–0.27)	0.24 (0.20–0.28)	0.11 (0.09–0.13)	0.09 (0.07–0.12)
CIS	0.36 (0.25–0.46)	2.85 (2.16–3.36)	2.66 (1.98–3.17)	5.58 (4.21–6.71)	5.01 (4.46–5.77)	1.92 (1.50–2.24)	1.30 (1.10–1.49)	1.50 (1.35–1.66)	0.81 (0.74–0.89)	0.49 (0.44–0.54)
SAS	0.69 (0.43–0.92)	8.96 (6.58–10.86)	7.25 (5.39–8.55)	10.34 (7.52–12.59)	6.97 (5.11–8.38)	2.89 (2.08–3.54)	1.61 (1.17–1.96)	1.61 (1.16–1.94)	0.74 (0.53–0.91)	0.46 (0.33–0.56)
EAS	3.42 (2.45–4.36)	27.02 (21.21–31.03)	25.81 (20.34–29.44)	54.46 (44.75–61.82)	50.80 (43.93–59.93)	17.32 (14.56–19.20)	10.64 (9.22–12.06)	10.78 (9.20–12.12)	5.27 (4.54–5.94)	3.01 (2.52–3.47)
SEA	0.87 (0.61–1.16)	6.14 (5.04–6.87)	6.84 (5.42–8.57)	11.34 (8.24–16.15)	5.03 (4.12–5.70)	2.13 (1.65–2.48)	1.16 (0.89–1.39)	1.17 (0.89–1.39)	0.55 (0.41–0.67)	0.33 (0.25–0.40)
PAN	0.34 (0.27–0.43)	1.44 (1.13–1.70)	2.13 (1.66–2.65)	2.11 (1.74–2.39)	0.60 (0.42–0.77)	0.30 (0.21–0.37)	0.15 (0.10–0.19)	0.15 (0.10–0.19)	0.07 (0.05–0.09)	0.04 (0.03–0.06)
ARC	0.02 (0.01–0.02)	0.13 (0.09–0.16)	0.12 (0.08–0.15)	0.25 (0.17–0.31)	0.21 (0.16–0.26)	0.09 (0.06–0.11)	0.06 (0.05–0.07)	0.09 (0.07–0.11)	0.06 (0.04–0.09)	0.02 (0.01–0.02)
Anthr	14.54 (10.50–18.82)	101.46 (79.71–117.79)	95.53 (73.89–112.46)	171.83 (134.01–204.93)	113.97 (93.91–135.66)	49.46 (39.65–58.00)	30.49 (24.71–35.98)	30.98 (25.09–36.60)	13.60 (11.22–15.78)	11.03 (8.63–13.73)
Full	135.66 (107.39–167.97)	631.57 (579.86–687.63)	602.52 (557.53–652.20)	985.28 (843.78–1125.06)	764.54 (650.09–889.18)	264.36 (247.81–282.65)	181.95 (160.85–204.76)	172.17 (153.88–191.98)	67.37 (59.95–75.32)	63.09 (56.09–70.92)

Appendix C. Model comparison with observation and Hg concentrations in sharks

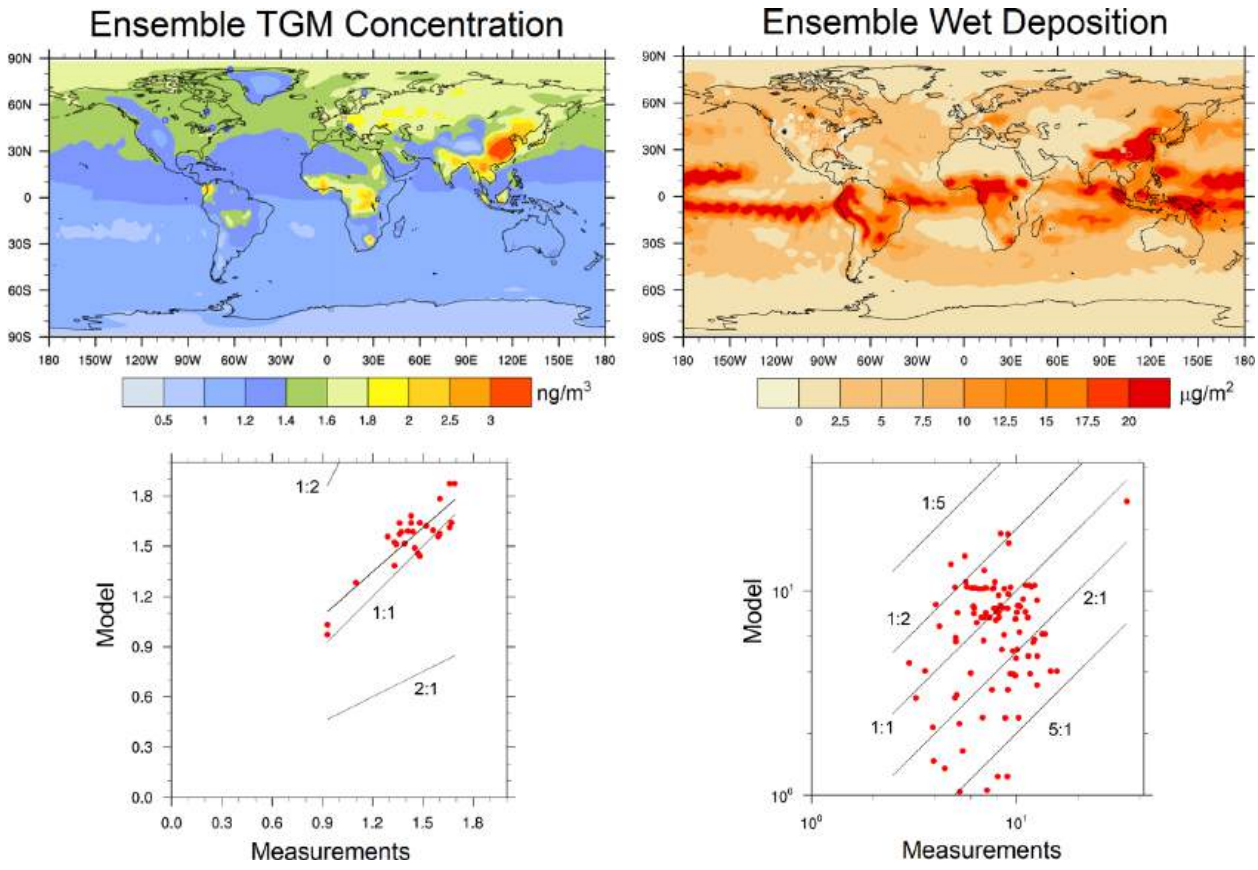

Fig. C.9: Comparison of Hg surface concentration and wet-deposition measurements from different measurement network with ensemble modelled values.

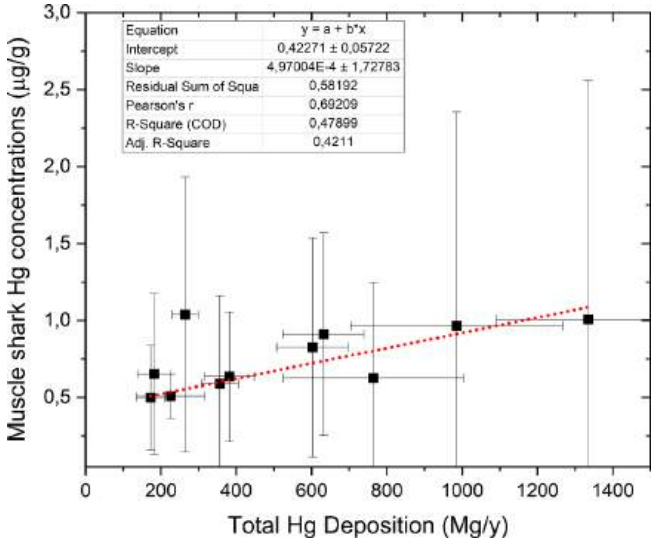

Fig. C.10: Comparison of Hg concentrations in sharks, as sampled in the different FAO fishery zones, against the Hg deposition over the same FAO zones as calculated in this study (*Full* set). The data of Hg concentrations in sharks were obtained from the review of Amezcua et al. (2022), in particular from "Table B.3: Estimated hazard quotients for Hg (HQ_{Hg}) in muscle of all shark species according to FAO region". The hazard quotients have been converted into the corresponding concentrations using the info reported in the section "Human Health Risk Assessment". Shark data from

Mediterranean sea (FAO 37) were discarded for the particular conditions that can enhance the biomagnification, resulting in the so called "Mediterranean Hg anomaly" (Cossa and Coquery, 2005; Tesán-Onrubia et al., 2023). Shark data from Pacific southeast (FAO 87) were also excluded due the very low number of samples (3) available. For visualisation purposes, in the plot are reported both Y errors bars, representing the SE for the Hg concentrations, and X error bars, representing the amplitude of the CI at 95% level of confidence of the Hg deposition. Fitting outcomes demonstrate a good Pearson correlation and that at the 95% level of confidence the slope of is statistically different from zero. These results confirm a good proportionality between total Hg deposition and Hg concentrations in fishes, at least for this published set, and therefore the rationale for considering the total Hg deposition as a measure of the Hg marine ecosystem. concentrations.

Appendix D. FAO statistics

Table D.5: FAO, 2023, Fishery and Aquaculture Statistics, Global production by zone of production source for years 2012–2021, in *Mg* - live weight

FAO ZONE	2012	2013	2014	2015	2016	2017]	2018	2019	2020	2021	Average *Mg −LW*
18	1	7	4	15	52	418	248	708	420	4236	611
21	2127101	1967358	1923989	1945933	1892439	1891186	1873687	1862622	1666848	1758583	1890975
27	10433234	10739189	11071275	11583714	10730216	11788153	11798472	10922267	10948845	10833260	11084863
31	1557334	1374017	1330695	1547698	1715659	1575724	1601393	1499412	1395365	1426707	1502400
34	4244233	4318802	4581167	4453201	4897564	5414274	5505738	5400604	4979094	5299386	4909406
37	1732445	1721492	1625581	1840758	1839476	2011442	1987236	2136967	1980704	2005225	1888133
41	1969527	2045807	2489060	2505442	1626736	1882968	1826761	1740509	1795951	2053171	1993593
47	1669435	1393802	1597086	1714615	1736023	1717974	1612690	1382230	1387622	1467188	1567867
48	153302	233532	285372	238874	259756	256048	314317	373928	462916	358991	293704
51	4743578	4742998	5030514	4971229	5290469	5726480	5794237	5857780	5419953	5727037	5330428
57	7037475	7112499	7302922	7443502	7495537	8390190	8011417	8086423	7947715	7704510	7653219
58	10878	11255	11999	11465	12457	12173	12120	11564	10767	10517	11520
61	52262419	53813533	55246663	56443907	58374691	59866426	61114463	62178793	63195296	64400548	58689674
67	3036703	3339712	3255490	3294436	3236945	3499941	3215355	3302901	2980384	3030588	3219246
71	23450652	26686861	28217679	29394088	29647168	28864746	29362852	29301675	29416706	29207233	28354966
77	2163485	2202949	2113069	1911411	1887554	2041990	2006043	2158232	2013271	2021515	2051952
81	707665	688042	688891	646142	587981	593287	563736	588488	547317	511191	612274
87	10048491	10438481	8893353	9562419	8176007	9365719	12531529	10421570	11244510	12882291	10356437
88	3615	4351	2536	4677	5131	2327	4402	3607	3171	2327	3614
Total	127351573	132834686	135667345	139513525	139411861	144901467	149136698	147230281	147396855	150704503	141414879

Table D.6: FAO, 2023, Fishery and Aquaculture Statistics, Global production by zone of production for years 2012–2021, in *Mg* - live weight. Countries are grouped by World Bank Classification.

FAO ZONE	2012	2013	2014	2015	2016	2017	2018	2019	2020	2021	Average *Mg −LW*
High income countries											
21	2108998	1950026	1909702	1928322	1877274	1876203	1857977	1844677	1649079	1744883	1874714
27	9465800	9712712	10041829	10520727	9665722	10656713	10709674	9851546	9864321	9683394	10017244
31	961841	801372	727605	862231	959165	807033	890352	854548	745232	700418	830980
34	478685	493525	618834	450479	556146	458869	310854	356584	289249	265579	427881
37	703980	715906	719393	736738	774415	792116	804942	752790	684840	700557	738568
41	399933	404416	642964	613826	213092	336353	281483	278887	291235	356740	381893
47	89598	67323	105929	146373	105082	103565	92455	56953	61805	47865	87695
48	148715	193901	225011	190838	187150	209104	258243	297155	327344	289741	232720
51	698121	744860	775090	832517	941775	1034004	1311570	1310705	1458877	1640099	1074762
57	191209	185278	181258	191441	215473	203758	207425	190708	210637	226162	200335
58	10616	11052	11693	11126	12194	11568	11530	11280	10477	10133	11167
61	7847139	7792853	7884973	7710059	7451547	7890089	8042666	7833173	7807330	7762752	7802258
67	3026111	3329561	3249101	3287507	3225915	3487953	3207627	3295993	2975278	3025476	3211052
71	971823	940664	1007803	899390	850569	770368	876392	905696	818454	807832	884899
77	535308	532263	531412	404771	382277	400510	375944	488298	392129	330161	437307
81	625093	613105	614552	589147	581870	586259	558386	577683	543999	508093	579819
87	4107227	3399395	3847069	3309514	2981390	3788764	3749587	3884265	3741362	3970338	3677891
88	3185	3757	2119	3497	3867	1646	3505	2716	2533	1882	2871
Total	32373381	31891970	33096337	32688501	30984924	33414875	33550613	32793657	31874182	32072106	32474054
Middle upper income countries											

(*continued on next page*)

(*continued*)

FAO ZONE	2012	2013	2014	2015	2016	2017	2018	2019	2020	2021	Average *Mg –LW*
18	1	7	4	15	52	418	248	708	420	4236	611
21	14360	14290	11683	14025	12135	11689	12425	14614	15076	11212	13151
27	957455	1015035	1021010	1052143	1049500	1120496	1074278	1053648	1064079	1126280	1053392
31	545571	518996	546093	626574	698789	710523	650128	586498	598761	662332	614427
34	419279	342645	380817	393318	401370	425684	574591	583357	437690	467501	442625
37	593073	557361	504816	703328	634286	741955	713786	911202	830256	828163	701823
41	1480692	1575183	1761371	1824717	1354363	1475990	1449838	1374425	1437979	1581184	1531574
47	1220919	938923	1061291	1099405	1151627	1091978	1074115	920434	936734	904588	1040001
48	4587	34979	51433	35471	65125	38931	40617	54620	114208	47605	48758
51	143634	151238	159601	161606	167699	196256	222601	259061	241810	220183	192369
57	1386972	1345442	1278552	1244255	1301645	1218825	1264160	1304879	1412548	1297805	1305508
58	263	203	306	339	263	605	590	284	291	384	353
61	43701261	45308491	46576625	47949982	50098463	51152755	52195270	53476359	54522472	55766380	50074806
67	10592	10151	6389	6929	11030	11988	7728	6908	5106	5112	8193
71	3127335	2978724	2795231	2664502	2612867	2540540	2555468	2606181	2469686	2413841	2676438
77	1498575	1548099	1442468	1396261	1408968	1516632	1504619	1541031	1494602	1556489	1490774
81	3518	5044	5481	6748	6108	7025	5347	10802	3315	3095	5648
87	5920386	7013512	5018383	6225517	5169796	5567696	8773427	6531507	7493341	8900791	6661436
88	430	482	301	919	797	435	351	407	91	0	421
Total	61028902	63358805	62621855	65406054	66144883	67830420	72119588	71236927	73078466	75797181	67862308
					Middle lower income countries						
21	0	0	0	85	0	44	0	0	0	0	13
27	9978	11441	8436	9113	10994	9360	13199	14269	18217	23584	12859
31	42605	46195	49227	50035	49287	50503	53918	51030	44398	57282	49448
34	2898511	2975466	3098859	3103033	3461338	3845993	3955717	3750272	3576940	3884237	3455036
37	433087	446222	399873	399269	429096	475805	466934	471395	464063	474725	446047
41	2079	5157	12973	13344	237	3013	2880	1611	1660	5940	4889
47	358239	386981	428768	462688	471856	518145	440512	400907	383913	514221	436623
48	0	4651	8929	12566	7481	8014	15457	22153	21363	21645	12226
51	3348121	3313946	3577667	3449197	3645854	3943009	3716562	3717360	3136071	3300243	3514803
57	5453713	5575333	5836815	6002796	5977779	6967607	6539833	6590837	6324531	6180542	6144978
61	0	1509	1915	6616	7331	4437	8231	3465	2700	2700	3890
71	19351285	22767195	24414390	25829886	26183550	25553622	25930732	25789494	26128302	25985297	24793375
77	122997	119834	136618	107993	93760	120565	120909	122935	123773	129268	119865
81	79051	69890	68855	50244	0	0	0	0	0	0	26804
87	20878	25573	27878	27387	24821	9259	8515	5799	9807	11162	17108
88	0	112	116	260	468	246	546	484	546	445	322
Total	32120544	35749507	38071316	39524514	40363852	41509622	41273944	40942010	40236284	40591292	39038288
					Low income countries						
34	447302	492548	482657	464622	467146	628581	594476	665413	630851	645541	551914
37	2300	2000	1499	1422	1679	1565	1574	1580	1545	1780	1694
41	340	0	0	0	0	0	0	0	0	0	34
51	506963	493966	505517	516557	524822	549427	539459	566779	579096	562187	534477
61	714020	710680	783150	777250	817350	819145	868295	865795	862795	868715	808720
Total	1670925	1699194	1772823	1759851	1810997	1998718	2003804	2099567	2074287	2078223	1896839

Table D.7: FAO, 2023, Fishery and Aquaculture Statistics, Summary of 2012–2021 average global production (in *Mg* - live weight) and distribution (in fraction) by zone of production. Countries are grouped by World Bank Classification.

	2012–2021 Average Production. Mg -LW				**2012–2021 Average Distribution. fraction**			
	Income Countries				**Income Countries**			
FAO ZONE	**Low**	**Lower-Middle**	**Upper-Middle**	**High**	**Low**	**Lower-Middle**	**Upper-Middle**	**High**
18	0	0	611	0	n	n	9.00E-06	n
21	0	13	13151	1874714	n	3.30E-07	1.94E-04	5.77E-02
27	0	12859	1053392	10017244	n	3.29E-04	1.55E-02	3.08E-01
31	0	49448	614427	830980	n	1.27E-03	9.05E-03	2.56E-02
34	551914	3455036	442625	427881	2.91E-01	8.85E-02	6.52E-03	1.32E-02
37	1694	446047	701823	738568	8.93E-04	1.14E-02	1.03E-02	2.27E-02
41	34	4889	1531574	381893	1.79E-05	1.25E-04	2.26E-02	1.18E-02
47	0	436623	1040001	87695	n	1.12E-02	1.53E-02	2.70E-03
48	0	12226	48758	232720	n	3.13E-04	7.18E-04	7.17E-03
51	534477	3514803	192369	1074762	2.82E-01	9.00E-02	2.83E-03	3.31E-02
57	0	6144978	1305508	200335	n	1.57E-01	1.92E-02	6.17E-03
58	0	0	353	11167	n	n	5.20E-06	3.44E-04
61	808720	3890	50074806	7802258	4.26E-01	9.97E-05	7.38E-01	2.40E-01
67	0	0	8193	3211052	n	n	1.21E-04	9.89E-02
71	0	24793375	2676438	884899	n	6.35E-01	3.94E-02	2.72E-02
77	0	119865	1490774	437307	n	3.07E-03	2.20E-02	1.35E-02

(*continued on next page*)

(*continued*)

	2012–2021 Average Production. Mg -LW					2012–2021 Average Distribution. fraction		
81	0	26804	5648	579819	n	6.87E-04	8.32E-05	1.79E-02
87	0	17108	6661436	3677891	n	4.38E-04	9.82E-02	1.13E-01
88	0	322	421	2871	n	8.26E-06	6.21E-06	8.84E-05
TOTAL	**1896839**	**39038288**	**67862308**	**32474054**	1	1	1	1

Table D.8: FAO, 2023, Fishery and Aquaculture Statistics, Import–Export averaged over 2019–2021 (in *Mg* - live weight) by production countries. Countries are grouped by World Bank Classification. As claimed by FAO: *"Differences between figures given for total exports and total imports of any one commodity may be due to several factors, e.g. the time lapse between the dispatch of goods from the exporting country and their arrival in the importing country; the use of a different classification of the same product by different countries; or the fact that some countries supply trade data on general trade, while others give data on special trade."*

IMPORT, *Mg* -LW	Country partner 2			
Country partner 1	High income	Upper-Middle income	Lower-Middle income	Low income
High income		6222458	3526945	119890
Upper-Middle income	3259224		3169130	37862
Lower-Middle income	2284893	1211395		81386
Low income	66182	338743	275383	

EXPORT, *Mg* -LW	Country partner 2			
Country partner 1	High income	Upper-Middle income	Lower-Middle income	Low income
High income		3400940	2216244	69425
Upper-Middle income	5686019		1196780	329734
Lower-Middle income	3492709	2967581		220970
Low income	86650	36026	60315	

Averaged over 2019–2021

Table D.9: FAO, 2023, Fishery and Aquaculture Statistics. Details of fish consumption calculation (in *Mg* - live weight) by FAO zones in countries classified by World Bank as having high income.

Mg-year	**Production**	**Export**	**Import from**				**consumption**
FAO ZONE	**High**	**High**	**Low**	**Lower-Middle**	**Upper-Middle**	**Total**	**High**
18	0	0	0	0	56	56	**56**
21	1874714	−328286	0	1	1206	1207	**1547635**
27	10017244	−1754143	0	1162	96588	97750	**8360850**
31	830980	−145515	0	4467	56338	60806	**746271**
34	427881	−74927	34884	312148	40585	387617	**740571**
37	738568	−129332	107	40298	64352	104757	**713993**
41	381893	−66874	2	442	140434	140878	**455896**
47	87695	−15356	0	39447	95360	134807	**207146**
48	232720	−40752	0	1105	4471	5575	**197543**
51	1074762	−188204	33782	317548	17639	368968	**1255526**
57	200335	−35081	0	555173	119705	674878	**840132**
58	11167	−1955	0	0	32	32	**9244**
61	7802258	−1366272	51115	351	4591479	4642946	**11078932**
67	3211052	−562295	0	0	751	751	**2649509**
71	884899	−154957	0	2239977	245409	2485386	**3215329**
77	437307	−76578	0	10829	136693	147522	**508251**
81	579819	−101533	0	2422	518	2940	**481225**
87	3677891	−644044	0	1546	610803	612349	**3646195**
88	2871	−503	0	29	39	68	**2436**
Total	**32474054**	**−5686609**	119890	3526945	6222458	**9869293**	**36656739**
%	100	−18	≤ 1	11	19	30	

Table D.10: FAO, 2023, Fishery and Aquaculture Statistics. Details of fish consumption calculation (in *Mg* - live weight) by FAO zones in countries classified by World Bank as having Upper-middle income.

Mg-year	**Production**	**Export**	**Import**				**consumption**
FAO ZONE	**Upper-Middle**	**Upper-Middle**	**Low**	**Lower-Middle**	**High**	**Total**	**Upper-Middle**
18	611	−65	0	0	0	0	**546**
21	13151	−1398	0	1	188154	188155	**199908**
27	1053392	−111957	0	1044	1005370	1006414	**1947850**
31	614427	−65302	0	4014	83400	87415	**636539**

(*continued on next page*)

(*continued*)

Mg-year	Production	Export			Import		consumption
34	442625	−47043	11016	280480	42944	334440	**730022**
37	701823	−74591	34	36210	74126	110369	**737601**
41	1531574	−162779	1	397	38328	38726	**1407522**
47	1040001	−110533	0	35445	8801	44246	**973714**
48	48758	−5182	0	992	23357	24349	**67925**
51	192369	−20445	10668	285332	107867	403868	**575791**
57	1305508	−138752	0	498850	20106	518956	**1685712**
58	353	−37	0	0	1121	1121	**1436**
61	50074806	−5322044	16142	316	783065	799524	**45552285**
67	8193	−871	0	0	322274	322274	**329596**
71	2676438	−284457	0	2012728	88812	2101539	**4493520**
77	1490774	−158442	0	9731	43890	53621	**1385953**
81	5648	−600	0	2176	58193	60369	**65417**
87	6661436	−707990	0	1389	369128	370516	**6323962**
88	421	−45	0	26	288	314	**691**
Total	**67862308**	**−7212534**	37862	3169130	3259224	**6466216**	**67115990**
%	100	−11	≤ 1	5	5	10	

Table D.11: FAO, 2023, Fishery and Aquaculture Statistics. Details of fish consumption calculation (in *Mg* - live weight) by FAO zones in countries classified by World Bank as having Lower-middle income.

Mg-year	Production	Export		Import			consumption
FAO ZONE	**Lower Middle**	**Lower Middle**	**Low**	**Upper-Middle**	**High**	**Total**	**Lower Middle**
18	0	0	0	11	0	11	**11**
21	13	−2	0	235	131906	132141	**132151**
27	12859	−2201	0	18804	704819	723623	**734281**
31	49448	−8463	0	10968	58468	69436	**110421**
34	3455036	−591317	23680	7901	30106	61687	**2925407**
37	446047	−76339	73	12528	51966	64567	**434274**
41	4889	−837	1	27340	26870	54211	**58264**
47	436623	−74726	0	18565	6170	24735	**386632**
48	12226	−2092	0	870	16374	17245	**27378**
51	3514803	−601546	22932	3434	75621	101987	**3015244**
57	6144978	−1051690	0	23304	14096	37400	**5130688**
58	0	0	0	6	786	792	**792**
61	3890	−666	34699	893874	548971	1477545	**1480769**
67	0	0	0	146	225931	226078	**226078**
71	24793375	−4243295	0	47777	62262	110039	**20660119**
77	119865	−20515	0	26611	30769	57381	**156732**
81	26804	−4587	0	101	40796	40897	**63114**
87	17108	−2928	0	118912	258779	377690	**391870**
88	322	−55	0	8	202	210	**477**
Total	**39038288**	**−6681259**	81386	1211395	2284893	**3577674**	**35934703**
%	100	−17	≤ 1	3	6	9	

Table D.12: FAO, 2023, Fishery and Aquaculture Statistics. Details of fish consumption calculation (in *Mg* - live weight) by FAO zones in countries classified by World Bank as having Low income.

Mg-year	Production	Export		Import			consumption
FAO ZONE	**Low**	**Low**	**Lower Middle**	**Upper-Middle**	**High**	**Total**	**Low**
18	0	0	0	3	0	3	**3**
21	0	0	0	66	3821	3886	**3886**
27	0	0	91	5258	20415	25764	**25764**
31	0	0	349	3067	1694	5109	**5109**
34	551914	−53244	24372	2209	872	27454	**526124**
37	1694	−163	3146	3503	1505	8155	**9686**
41	34	−3	34	7645	778	8458	**8489**
47	0	0	3080	5191	179	8450	**8450**
48	0	0	86	243	474	804	**804**
51	534477	−51562	24794	960	2190	27945	**510860**
57	0	0	43348	6517	408	50273	**50273**
58	0	0	0	2	23	25	**25**
61	808720	−78019	27	249954	15901	265883	**996584**
67	0	0	0	41	6544	6585	**6585**
71	0	0	174897	13360	1803	190060	**190060**
77	0	0	846	7441	891	9178	**9178**
81	0	0	189	28	1182	1399	**1399**

(*continued on next page*)

(*continued*)

Mg-year	Production	Export		Import			consumption
87	0	0	121	33251	7496	40868	**40868**
88	0	0	2	2	6	10	**10**
Total	**1896839**	**−182991**	275383	338743	66182	**680308**	**2394156**
%	100	−10	15	18	3	36	

Table D.13: Differences between production and consumption distribution by FAO fishery zones for countries classified by World Bank as having High, Upper-middle, Lower-middle and Low income.

	Distribution by FAO Fishery Zone (%)							
	Low		Lower-Middle		Upper-Middle		High	
FAO ZONE	Consumption	Production	Consumption	Production	Consumption	Production	Consumption	Production
18	0.00	0.00	0.00	0.00	0.00	0.00	0.00	0.00
21	0.16	0.00	0.37	0.00	0.30	0.02	4.22	5.77
27	1.08	0.00	2.04	0.03	2.90	1.55	22.81	30.85
31	0.21	0.00	0.31	0.13	0.95	0.91	2.04	2.56
34	21.98	29.10	8.14	8.85	1.09	0.65	2.02	1.32
37	0.40	0.09	1.21	1.14	1.10	1.03	1.95	2.27
41	0.35	0.00	0.16	0.01	2.10	2.26	1.24	1.18
47	0.35	0.00	1.08	1.12	1.45	1.53	0.57	0.27
48	0.03	0.00	0.08	0.03	0.10	0.07	0.54	0.72
51	21.34	28.18	8.39	9.00	0.86	0.28	3.43	3.31
57	2.10	0.00	14.28	15.74	2.51	1.92	2.29	0.62
58	0.00	0.00	0.00	0.00	0.00	0.00	0.03	0.03
61	41.63	42.64	4.12	0.01	67.87	73.79	30.22	24.03
67	0.28	0.00	0.63	0.00	0.49	0.01	7.23	9.89
71	7.94	0.00	57.49	63.51	6.70	3.94	8.77	2.72
77	0.38	0.00	0.44	0.31	2.07	2.20	1.39	1.35
81	0.06	0.00	0.18	0.07	0.10	0.01	1.31	1.79
87	1.71	0.00	1.09	0.04	9.42	9.82	9.95	11.33
88	0.00	0.00	0.00	0.00	0.00	0.00	0.01	0.01
Total (%)	100.00	100.00	100.00	100.00	100.00	100.00	100.00	100.00

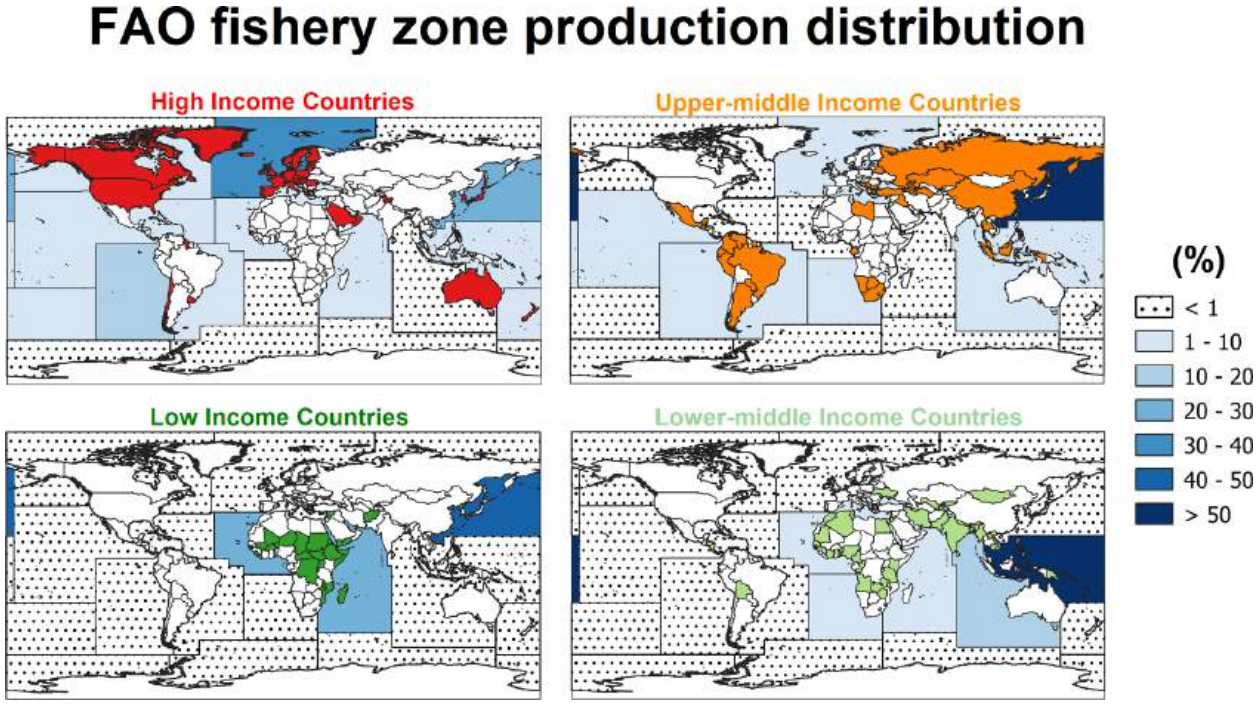

Fig. D.11: Geographical distribution of the production distribution, in percentage, by FAO fishery zone for the countries classified by World Bank as having High, Upper-middle, Lower-middle and Low Income, respectively. Each panel also reports the countries belonging to the relevant classification.

Appendix E. *OnlyAnthr_Src*$_{Rg\times Sx}$ $-Rcp$ **results: Hg$_{anthr}$ fingerprints over each FAO Fishery zone**

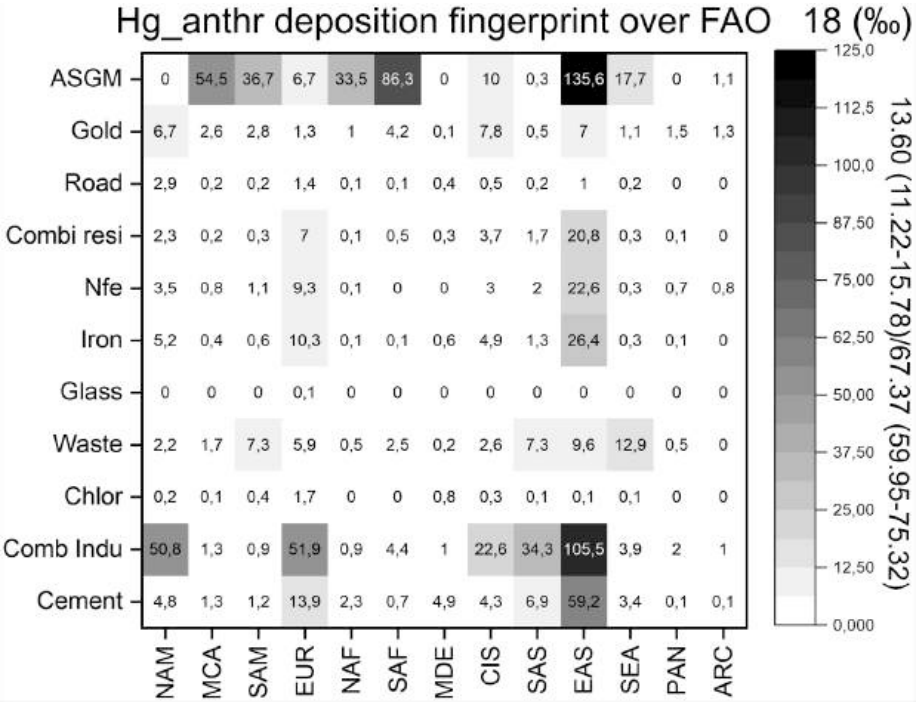

Fig. E.12: Heatmap illustrating the fingerprint (‰) of Hg$_{anthr}$ emissions in term of source sectors, on rows, and source regions, on columns, on the Hg$_{anthr}$ deposition, over FAO fishery zone 18. The side text-box reports in Mg/y the ratio of Hg$_{anthr}$ deposition to Hg deposition, calculated as means from *Full* and $S_R - R$ ensembles, respectively. In bracket, the CI at 95% level of confidence.

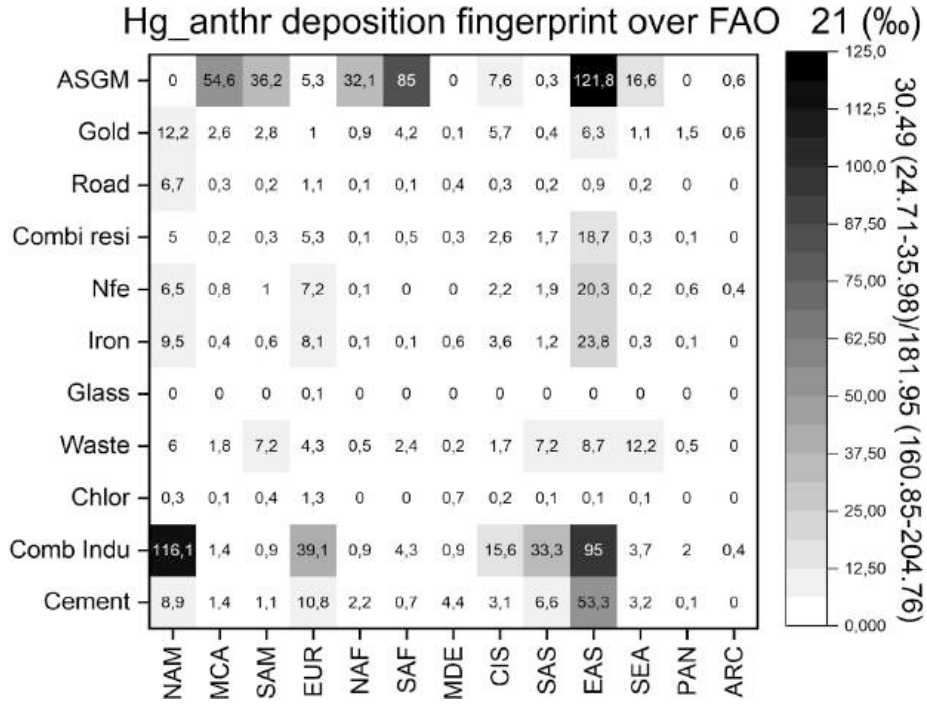

Fig. E.13: Heatmap illustrating the fingerprint (‰) of Hg$_{anthr}$ emissions in term of source sectors, on rows, and source regions, on columns, on the Hg$_{anthr}$ deposition, over FAO fishery zone 21. The side text-box reports in Mg/y the ratio of Hg$_{anthr}$ deposition to Hg deposition, calculated as means from *Full* and $S_R - R$ ensembles, respectively. In bracket, the CI at 95% level of confidence.

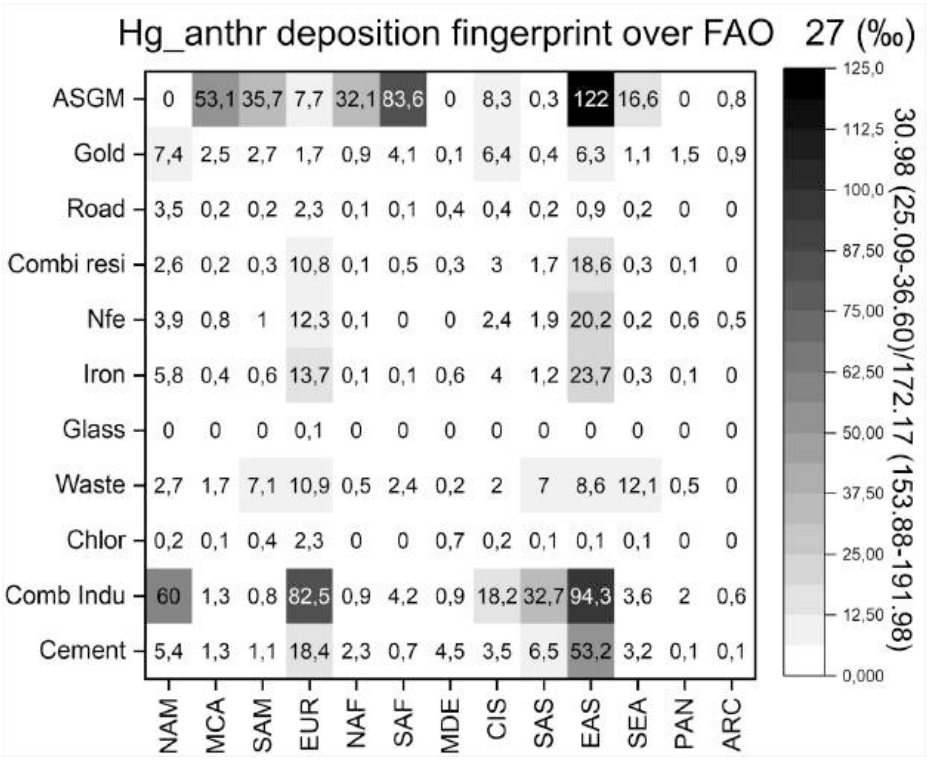

Fig. E.14: Heatmap illustrating the fingerprint (‰) of Hg_{anthr} emissions in term of source sectors, on rows, and source regions, on columns, on the Hg_{anthr} deposition, over FAO fishery zone 27. The side text-box reports in Mg/y the ratio of Hg_{anthr} deposition to Hg deposition, calculated as means from *Full* and $S_R - R$ ensembles, respectively. In bracket, the CI at 95% level of confidence.

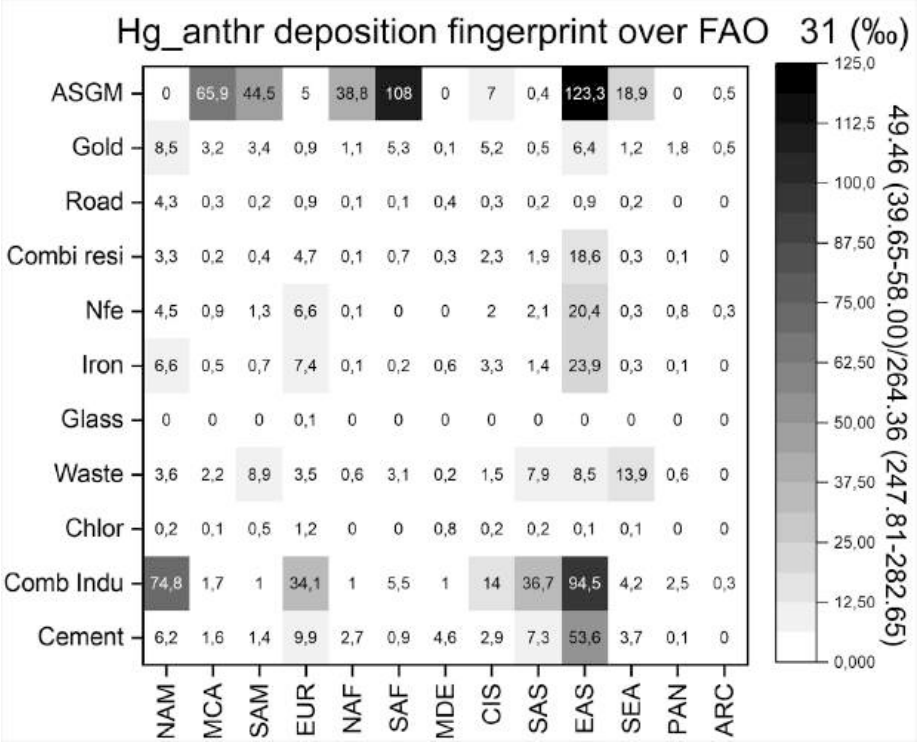

Fig. E.15: Heatmap illustrating the fingerprint (‰) of Hg_{anthr} emissions in term of source sectors, on rows, and source regions, on columns, on the Hg_{anthr} deposition, over FAO fishery zone 31. The side text-box reports in Mg/y the ratio of Hg_{anthr} deposition to Hg deposition, calculated as means

from *Full* and $S_R - R$ ensembles, respectively. In bracket, the CI at 95% level of confidence.

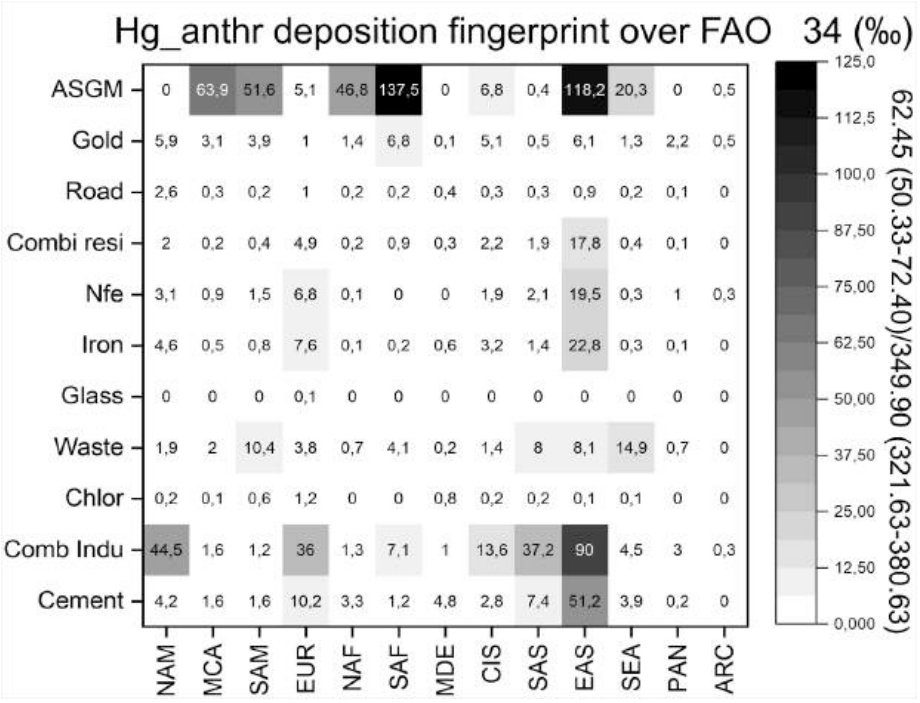

Fig. E.16: Heatmap illustrating the fingerprint (‰) of Hg_{anthr} emissions in term of source sectors, on rows, and source regions, on columns, on the Hg_{anthr} deposition, over FAO fishery zone 34. The side text-box reports in Mg/y the ratio of Hg_{anthr} deposition to Hg deposition, calculated as means from *Full* and $S_R - R$ ensembles, respectively. In bracket, the CI at 95% level of confidence.

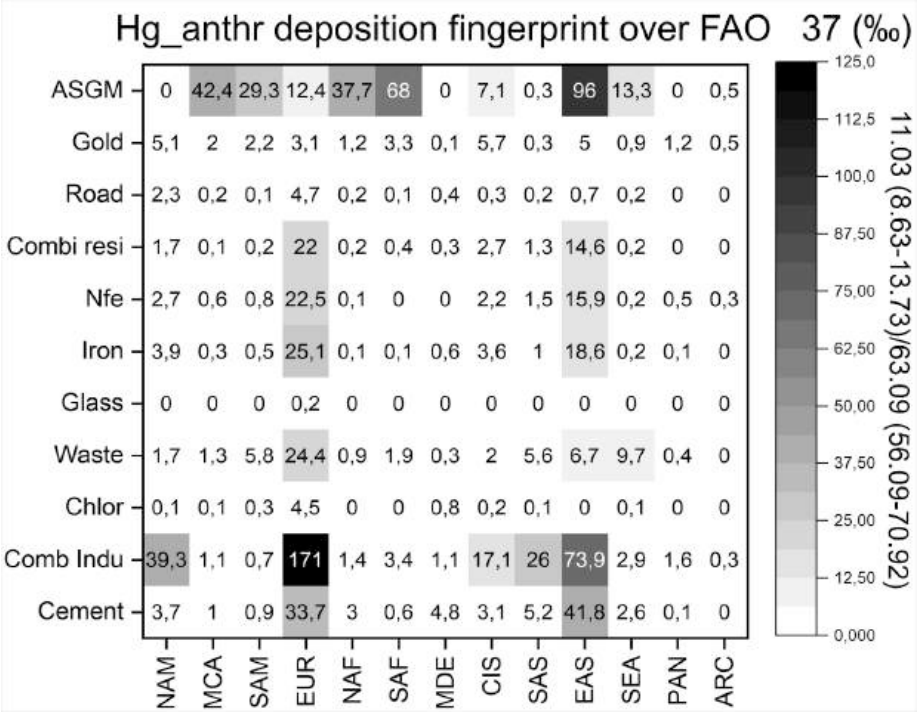

Fig. E.17: Heatmap illustrating the fingerprint (‰) of Hg_{anthr} emissions in term of source sectors, on rows, and source regions, on columns, on the Hg_{anthr} deposition, over FAO fishery zone 37. The side text-box reports in Mg/y the ratio of Hg_{anthr} deposition to Hg deposition, calculated as means from *Full* and $S_R - R$ ensembles, respectively. In bracket, the CI at 95% level of confidence.

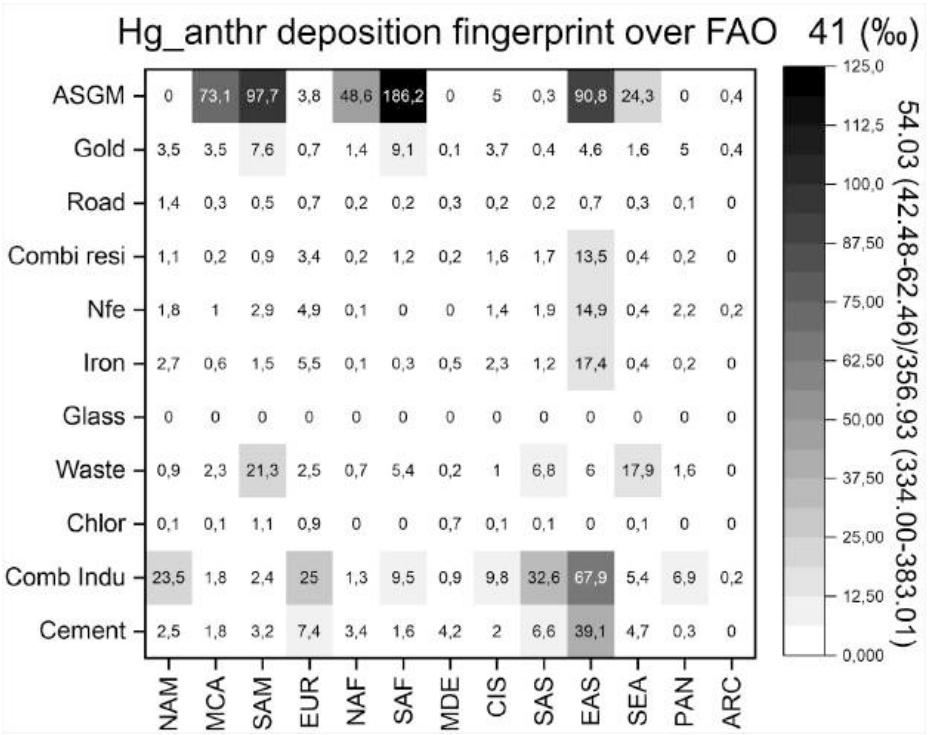

Fig. E.18: Heatmap illustrating the fingerprint (‰) of Hg_{anthr} emissions in term of source sectors, on rows, and source regions, on columns, on the Hg_{anthr} deposition, over FAO fishery zone 41. The side text-box reports in Mg/y the ratio of Hg_{anthr} deposition to Hg deposition, calculated as means from *Full* and $S_R - R$ ensembles, respectively. In bracket, the CI at 95% level of confidence.

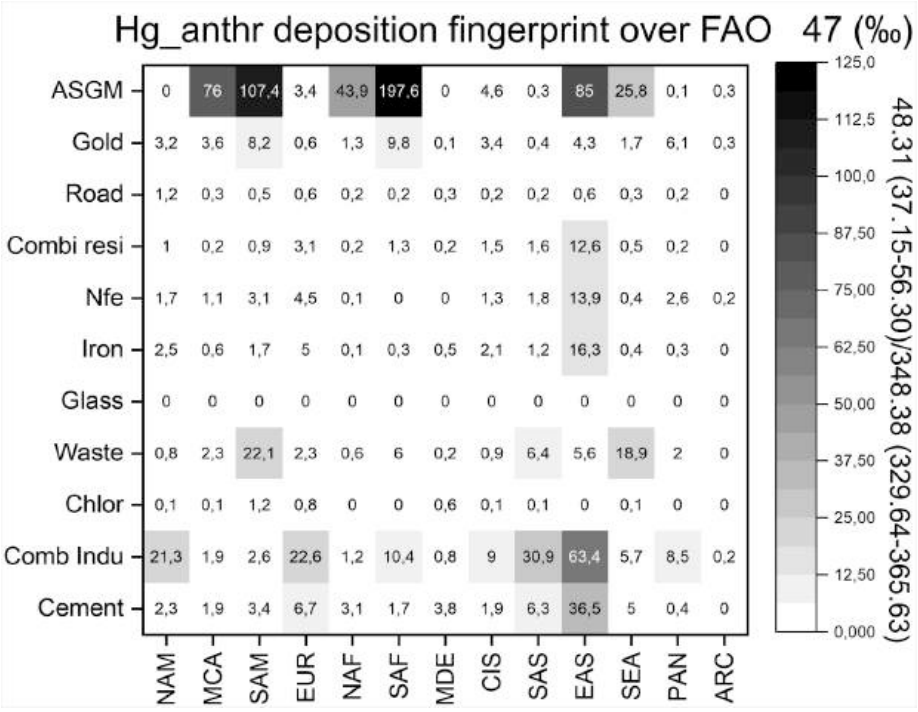

Fig. E.19: Heatmap illustrating the fingerprint (‰) of Hg_{anthr} emissions in term of source sectors, on rows, and source regions, on columns, on the Hg_{anthr} deposition, over FAO fishery zone 47. The side text-box reports in Mg/y the ratio of Hg_{anthr} deposition to Hg deposition, calculated as means from *Full* and $S_R - R$ ensembles, respectively. In bracket, the CI at 95% level of confidence.

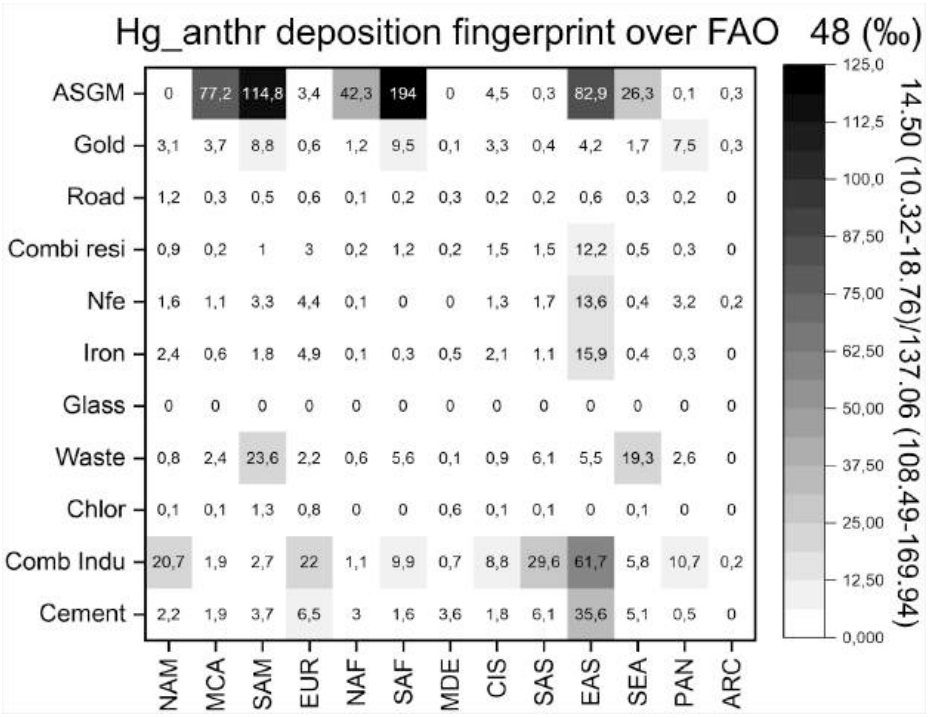

Fig. E.20: Heatmap illustrating the fingerprint (‰) of Hg_{anthr} emissions in term of source sectors, on rows, and source regions, on columns, on the Hg_{anthr} deposition, over FAO fishery zone 48. The side text-box reports in Mg/y the ratio of Hg_{anthr} deposition to Hg deposition, calculated as means from *Full* and $S_R - R$ ensembles, respectively. In bracket, the CI at 95% level of confidence.

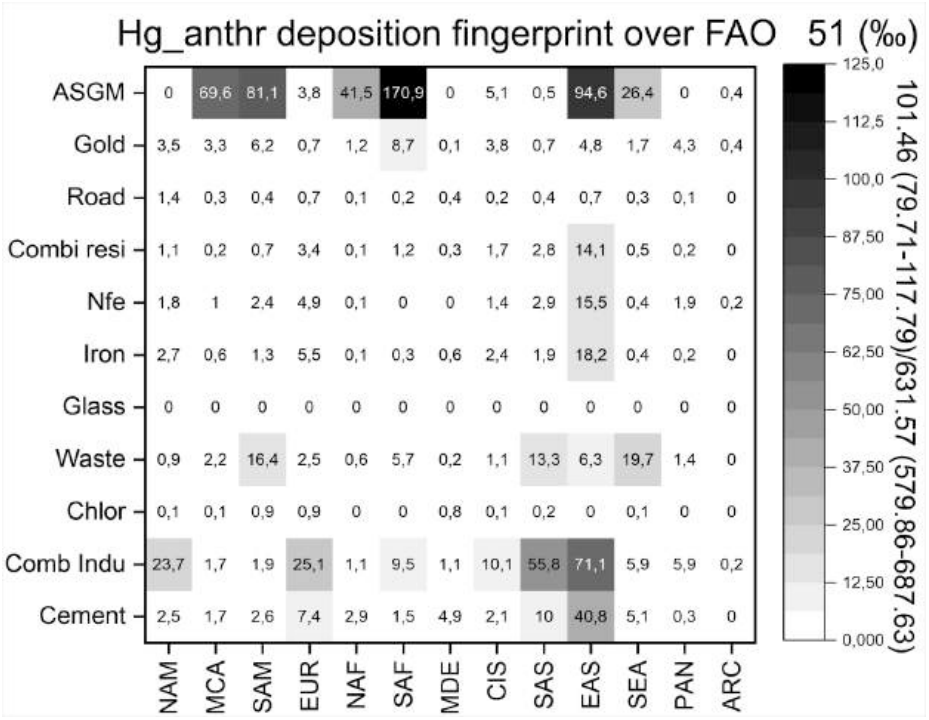

Fig. E.21: Heatmap illustrating the fingerprint (‰) of Hg_{anthr} emissions in term of source sectors, on rows, and source regions, on columns, on the Hg_{anthr} deposition, over FAO fishery zone 51. The side text-box reports in Mg/y the ratio of Hg_{anthr} deposition to Hg deposition, calculated as means from *Full* and $S_R - R$ ensembles, respectively. In bracket, the CI at 95% level of confidence.

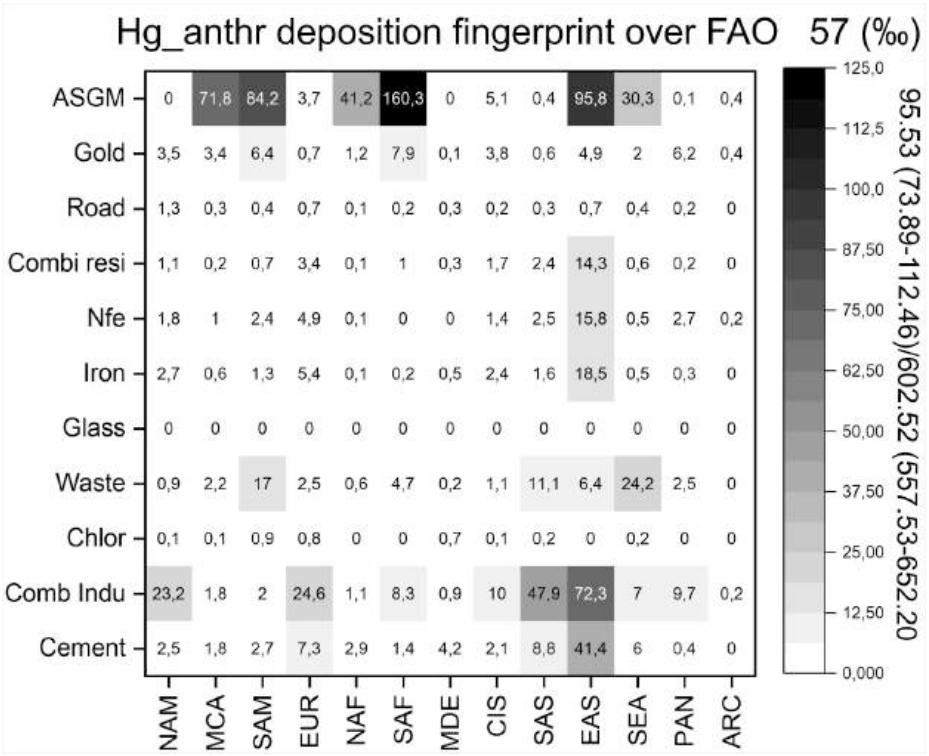

Fig. E.22: Heatmap illustrating the fingerprint (‰) of Hg_{anthr} emissions in term of source sectors, on rows, and source regions, on columns, on the Hg_{anthr} deposition, over FAO fishery zone 57. The side text-box reports in Mg/y the ratio of Hg_{anthr} deposition to Hg deposition, calculated as means from *Full* and $S_R - R$ ensembles, respectively. In bracket, the CI at 95% level of confidence.

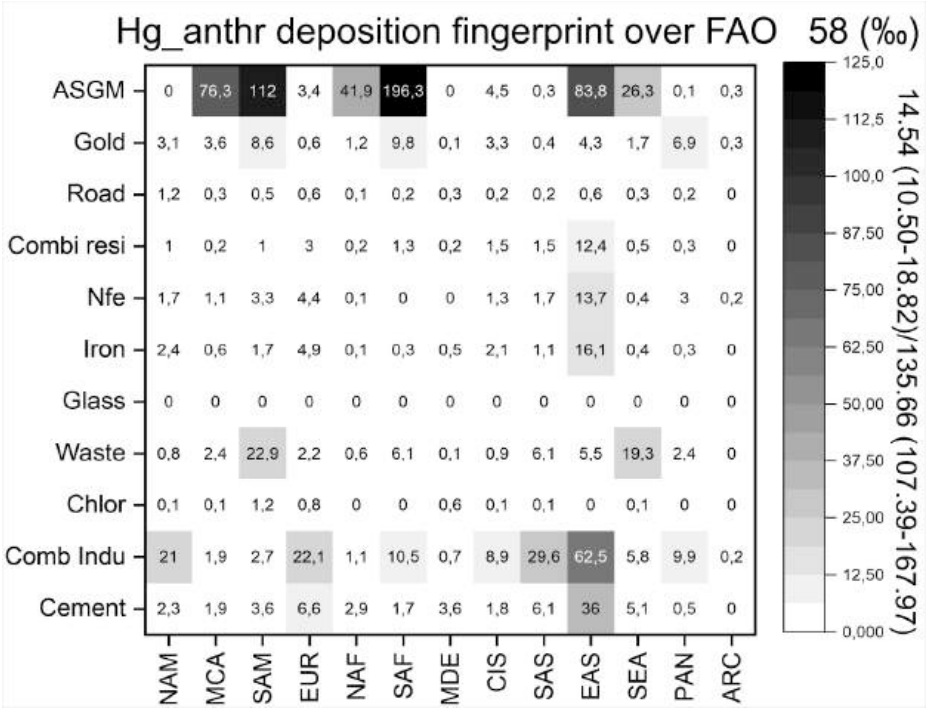

Fig. E.23: Heatmap illustrating the fingerprint (‰) of Hg_{anthr} emissions in term of source sectors, on rows, and source regions, on columns, on the Hg_{anthr} deposition, over FAO fishery zone 58. The side text-box reports in Mg/y the ratio of Hg_{anthr} deposition to Hg deposition, calculated as means from *Full* and $S_R - R$ ensembles, respectively. In bracket, the CI at 95% level of confidence.

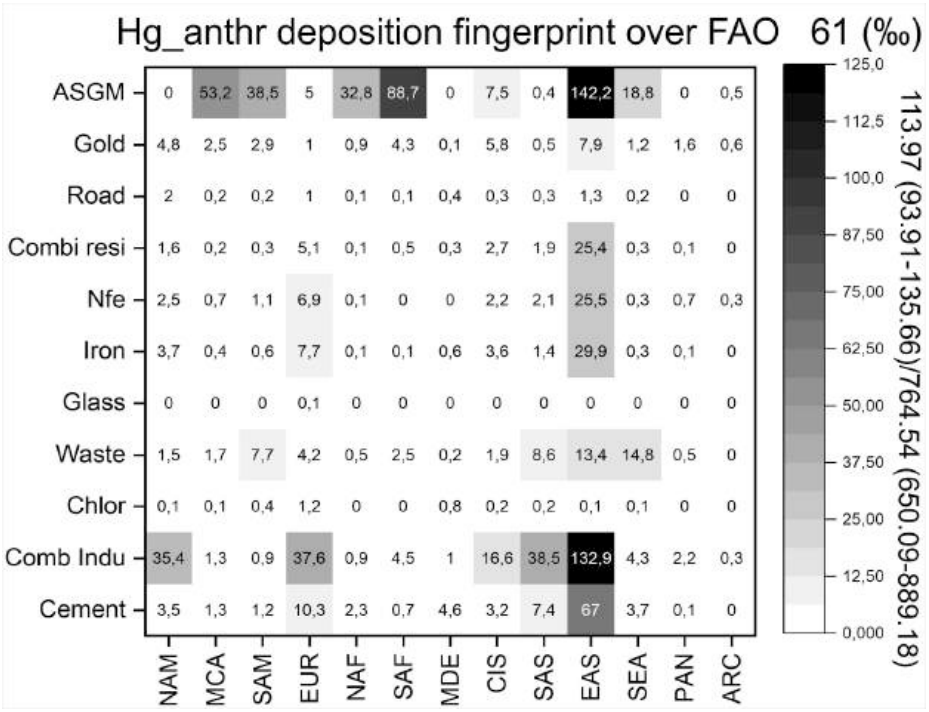

Fig. E.24: Heatmap illustrating the fingerprint (‰) of Hg_{anthr} emissions in term of source sectors, on rows, and source regions, on columns, on the Hg_{anthr} deposition, over FAO fishery zone 61. The side text-box reports in Mg/y the ratio of Hg_{anthr} deposition to Hg deposition, calculated as means from *Full* and $S_R - R$ ensembles, respectively. In bracket, the CI at 95% level of confidence.

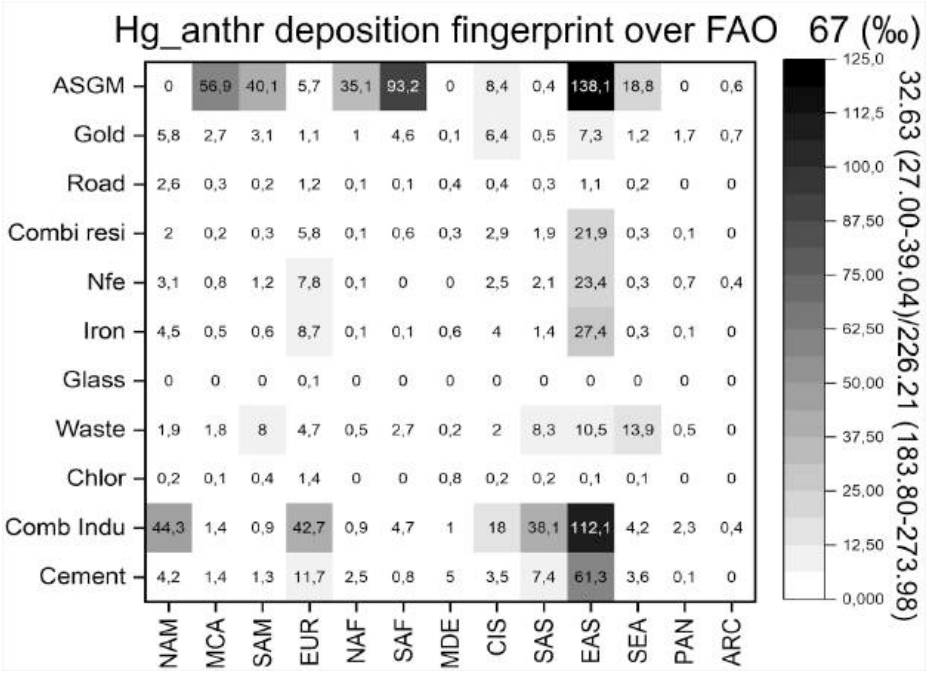

Fig. E.25: Heatmap illustrating the fingerprint (‰) of Hg_{anthr} emissions in term of source sectors, on rows, and source regions, on columns, on the Hg_{anthr} deposition, over FAO fishery zone 67. The side text-box reports in Mg/y the ratio of Hg_{anthr} deposition to Hg deposition, calculated as means from *Full* and $S_R - R$ ensembles, respectively. In bracket, the CI at 95% level of confidence.

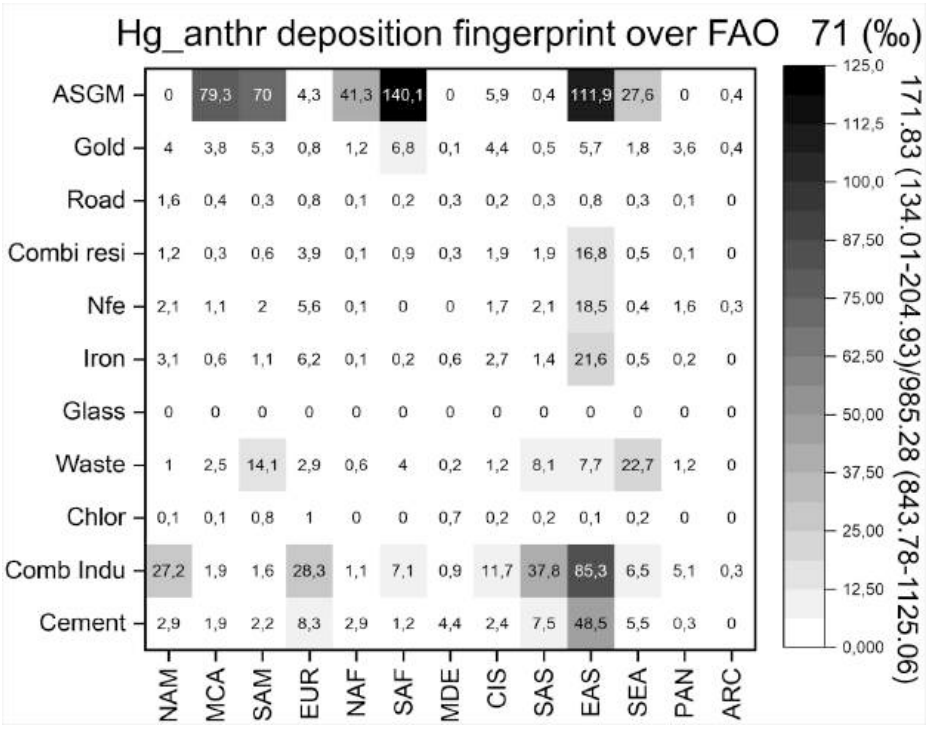

Fig. E.26: Heatmap illustrating the fingerprint (‰) of Hg_{anthr} emissions in term of source sectors, on rows, and source regions, on columns, on the Hg_{anthr} deposition, over FAO fishery zone 71. The side text-box reports in Mg/y the ratio of Hg_{anthr} deposition to Hg deposition, calculated as means from *Full* and $S_R - R$ ensembles, respectively. In bracket, the CI at 95% level of confidence.

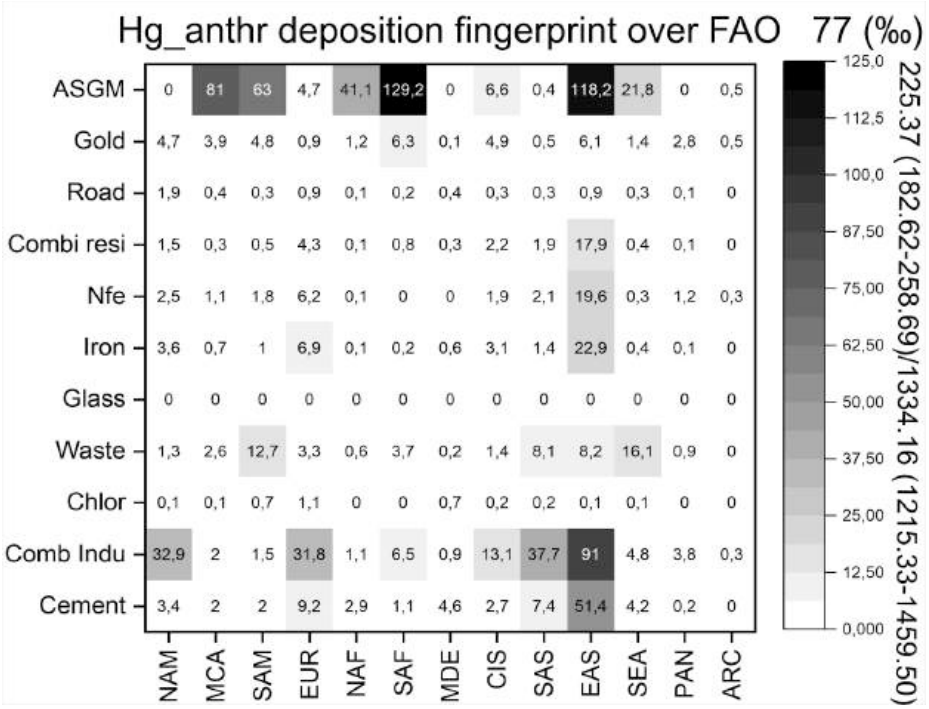

Fig. E.27: Heatmap illustrating the fingerprint (‰) of Hg_{anthr} emissions in term of source sectors, on rows, and source regions, on columns, on the Hg_{anthr} deposition, over FAO fishery zone 77. The side text-box reports in Mg/y the ratio of Hg_{anthr} deposition to Hg deposition, calculated as means from *Full* and $S_R - R$ ensembles, respectively. In bracket, the CI at 95% level of confidence.

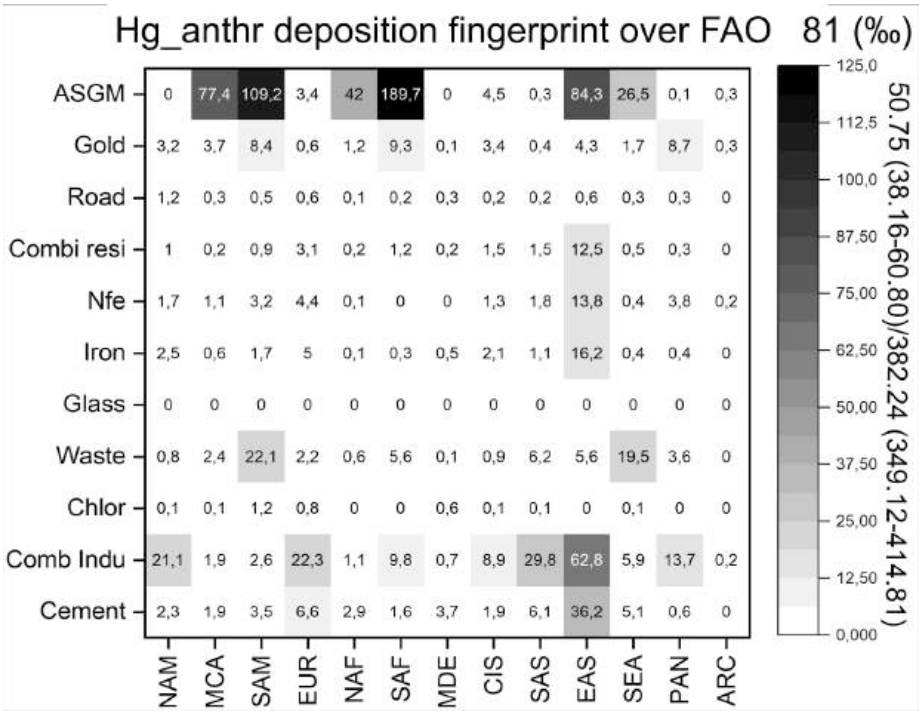

Fig. E.28: Heatmap illustrating the fingerprint (‰) of Hg_{anthr} emissions in term of source sectors, on rows, and source regions, on columns, on the Hg_{anthr} deposition, over FAO fishery zone 81. The side text-box reports in Mg/y the ratio of Hg_{anthr} deposition to Hg deposition, calculated as means from *Full* and $S_R - R$ ensembles, respectively. In bracket, the CI at 95% level of confidence.

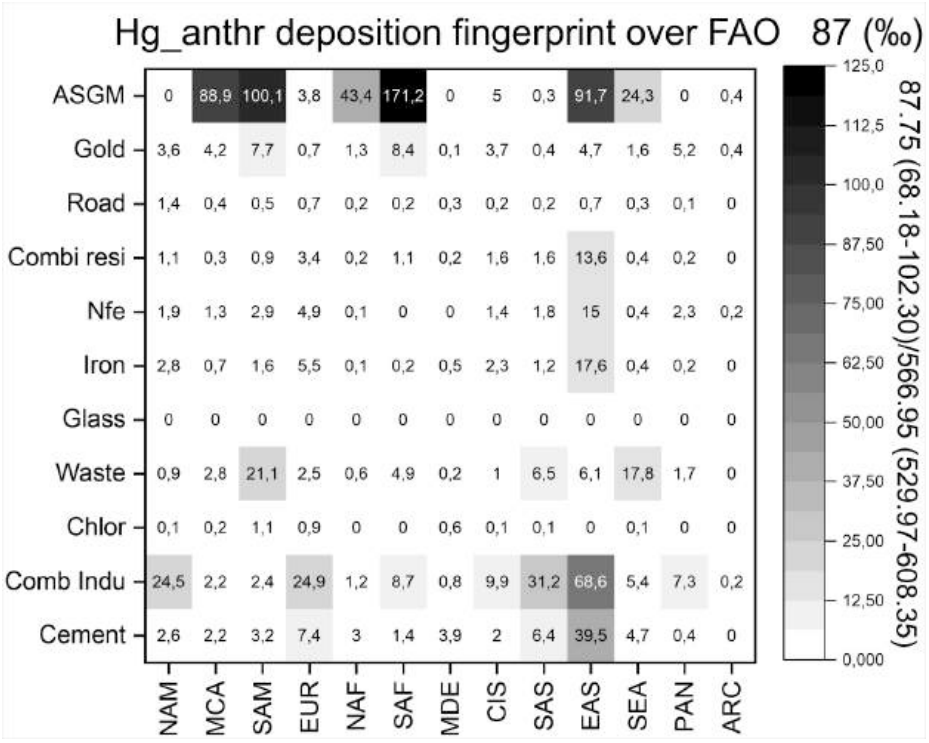

Fig. E.29: Heatmap illustrating the fingerprint (‰) of Hg_{anthr} emissions in term of source sectors, on rows, and source regions, on columns, on the Hg_{anthr} deposition, over FAO fishery zone 87. The side text-box reports in Mg/y the ratio of Hg_{anthr} deposition to Hg deposition, calculated as means from *Full* and $S_R - R$ ensembles, respectively. In bracket, the CI at 95% level of confidence.

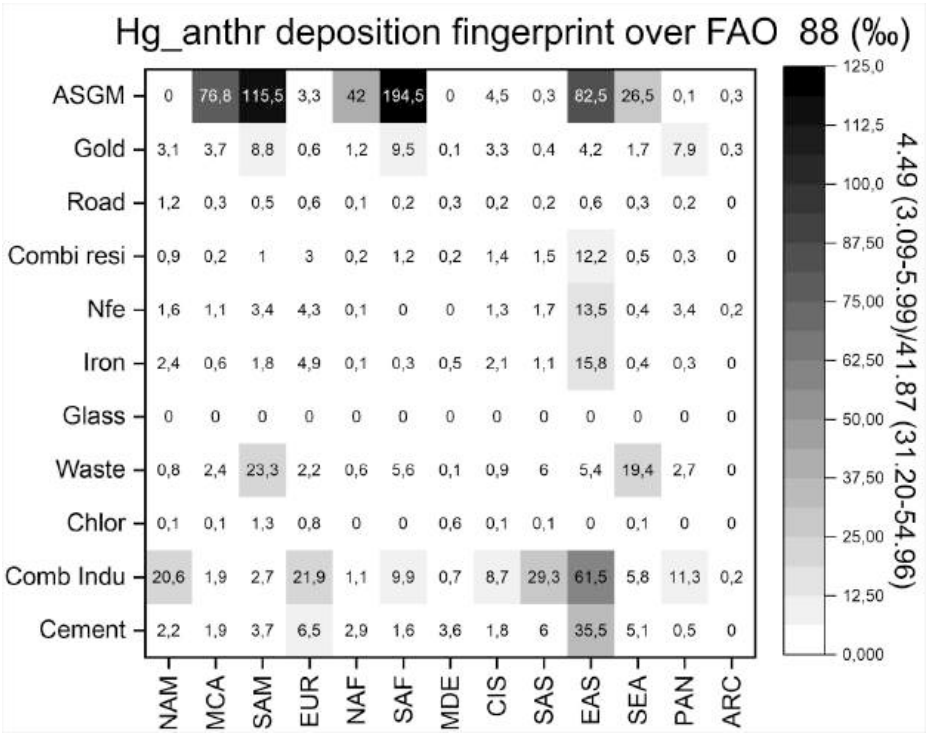

Fig. E.30: Heatmap illustrating the fingerprint (‰) of Hg_{anthr} emissions in term of source sectors, on rows, and source regions, on columns, on the Hg_{anthr} deposition, over FAO fishery zone 88. The side text-box reports in Mg/y the ratio of Hg_{anthr} deposition to Hg deposition, calculated as means from *Full* and $S_R - R$ ensembles, respectively. In bracket, the CI at 95% level of confidence.

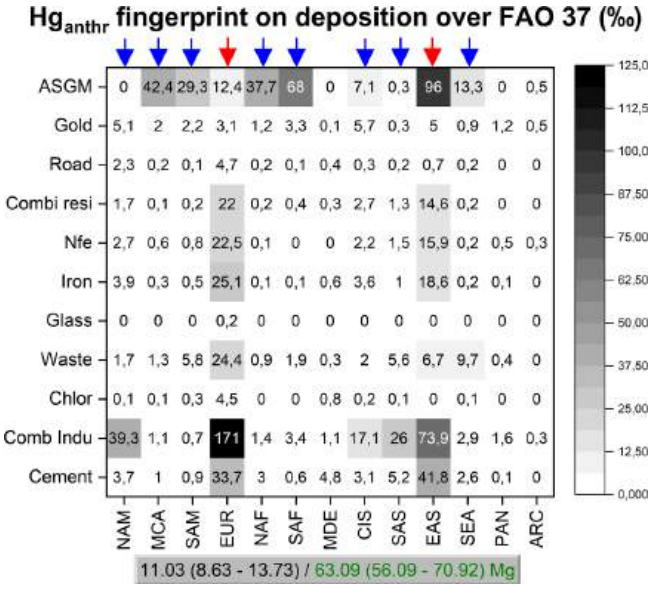

Fig. E.31: Heatmap illustrating the relative joint contributions (in ‰) of source-sectors, on rows, and source-regions, on columns, on the resulting deposition of Hg_{anthr}, over the FAO 37 fishery zone (Mediterranean Sea). The bottom marble box reports, in Mg/y the total deposition due to Hg_{anthr} primary emissions respect to the Hg deposition from all sources, with the relative C.I. (at 95% level of confidence). The top arrows of the same colours indicate the regions whose contributions are statistically indistinguishable (at 95% level of confidence).

References

AMAP/UNEP, 2013. Amap/unep technical background report for the global mercury assessment 2013: final technical report; output.

Amezcua, F., Ruelas-Inzunza, J., Coiraton, C., Spanopoulos-Zarco, P., Páez-Osuna, F., 2022. A global review of cadmium, mercury, and selenium in sharks: geographical patterns, baseline levels and human health implications. Rev. Environ. Contam. Toxicol. 260, 4.

Amos, H.M., Jacob, D.J., Streets, D.G., Sunderland, E.M., 2013. Legacy impacts of all-time anthropogenic emissions on the global mercury cycle. Global Biogeochem. Cycles 27, 410–421.

Angot, H., Dastoor, A., De Simone, F., Gårdfeldt, K., Gencarelli, C.N., Hedgecock, I.M., Langer, S., Magand, O., Mastromonaco, M.N., Nordstrøm, C., et al., 2016. Chemical cycling and deposition of atmospheric mercury in polar regions: review of recent measurements and comparison with models. Atmos. Chem. Phys. 16, 10735–10763.

Angot, H., Hoffman, N., Giang, A., Thackray, C.P., Hendricks, A.N., Urban, N.R., Selin, N. E., 2018. Global and local impacts of delayed mercury mitigation efforts. Environ. Sci. Technol. 52, 12968–12977.

Ariya, P.A., Amyot, M., Dastoor, A., Deeds, D., Feinberg, A., Kos, G., Poulain, A., Ryjkov, A., Semeniuk, K., Subir, M., et al., 2015. Mercury physicochemical and biogeochemical transformation in the atmosphere and at atmospheric interfaces: A review and future directions. Chem. Rev. 115, 3760–3802.

Axelrad, D.A., Bellinger, D.C., Ryan, L.M., Woodruff, T.J., 2007. Dose–response relationship of prenatal mercury exposure and iq: an integrative analysis of epidemiologic data. Environmental health perspectives 115, 609–615.

Bai, X., Tian, H., Zhu, C., Luo, L., Hao, Y., Liu, S., Guo, Z., Lv, Y., Chen, D., Chu, B., et al., 2023. Present knowledge and future perspectives of atmospheric emission inventories of toxic trace elements: A critical review. Environmental Science & Technology.

Bellanger, M., Pichery, C., Aerts, D., Berglund, M., Castaño, A., Čejchanová, M., Crettaz, P., Davidson, F., Esteban, M., Fischer, M.E., et al., 2013. Economic benefits of methylmercury exposure control in europe: monetary value of neurotoxicity prevention. Environmental Health 12, 1–10.

Bieser, J., Amptmeijer, D.J., Daewel, U., Kuss, J., Sørensen, A.L., Schrum, C., 2023. The 3d biogeochemical marine mercury cycling model mercy v2. 0–linking atmospheric hg to methylmercury in fish. Geoscientific Model Development 16, 2649–2688.

Chen, C.Y., Driscoll, C.T., Lambert, K.F., Mason, R.P., Rardin, L.R., Schmitt, C.V., Serrell, N., Sunderland, E.M., 2012. Sources to seafood: mercury pollution in the marine environment.

Cheung, W.W., Lam, V.W., Sarmiento, J.L., Kearney, K., Watson, R., Pauly, D., 2009. Projecting global marine biodiversity impacts under climate change scenarios. Fish and fisheries 10, 235–251.

Corbitt, E.S., Jacob, D.J., Holmes, C.D., Streets, D.G., Sunderland, E.M., 2011. Global source–receptor relationships for mercury deposition under present-day and 2050 emissions scenarios. Environmental science & technology 45, 10477–10484.

Cossa, D., Coquery, M., 2005. The mediterranean mercury anomaly, a geochemical or a biologocalissue. The Mediterranean Sea 177–208.

De Simone, F., Artaxo, P., Bencardino, M., Cinnirella, S., Carbone, F., D'Amore, F., Dommergue, A., Feng, X.B., Gencarelli, C.N., Hedgecock, I.M., et al., 2017. Particulate-phase mercury emissions from biomass burning and impact on resulting deposition: a modelling assessment. Atmospheric chemistry and physics 17, 1881–1899.

De Simone, F., Cinnirella, S., Gencarelli, C.N., Yang, X., Hedgecock, I.M., Pirrone, N., 2015. Model study of global mercury deposition from biomass burning. Environmental science & technology 49, 6712–6721.

De Simone, F., D'Amore, F., Bencardino, M., Carbone, F., Hedgecock, I.M., Sprovieri, F., Cinnirella, S., Pirrone, N., 2021. The gos4m knowledge hub: A web-based effectiveness evaluation platform in support of the minamata convention on mercury. Environmental Science & Policy 124, 235–246.

De Simone, F., D'Amore, F., Hedgecock, I.M., Bruno, D.E., Cinnirella, S., Sprovieri, F., Pirrone, N., 2022. Will action taken under the minamata convention on mercury need to be coordinated internationally? evidence from an optimization study suggests it will. Environmental Science & Policy 127, 22–30.

De Simone, F., D'Amore, F., Marasco, F., Carbone, F., Bencardino, M., Hedgecock, I.M., Cinnirella, S., Sprovieri, F., Pirrone, N., 2020. A chemical transport model emulator for the interactive evaluation of mercury emission reduction scenarios. Atmosphere 11, 878.

De Simone, F., Gencarelli, C., Hedgecock, I., Pirrone, N., 2014. Global atmospheric cycle of mercury: a model study on the impact of oxidation mechanisms. Environ. Sci. Pollut. Res. 21, 4110–4123.

De Simone, F., Gencarelli, C.N., Hedgecock, I.M., Pirrone, N., 2016. A modeling comparison of mercury deposition from current anthropogenic mercury emission inventories. Environmental Science & Technology 50, 5154–5162.

De Simone, F., Hedgecock, I.M., Carbone, F., Cinnirella, S., Sprovieri, F., Pirrone, N., 2017. Estimating uncertainty in global mercury emission source and deposition receptor relationships. Atmosphere 8, 236.

Drenner, R.W., Chumchal, M.M., Jones, C.M., Lehmann, C.M., Gay, D.A., Donato, D.I., 2013. Effects of mercury deposition and coniferous forests on the mercury contamination of fish in the south central united states. Environmental science & technology 47, 1274–1279.

FAO, F., Statistics, A., 2023. Global production by production source 1950–2015 (fishstatj). FAO Fisheries and Aquaculture Division. Rome. www.fao.org/fishery/en/statistics/software/fishstatj.

Gencarelli, C.N., De Simone, F., Hedgecock, I.M., Sprovieri, F., Pirrone, N., 2014. Development and application of a regional-scale atmospheric mercury model based on wrf/chem: a mediterranean area investigation. Environ. Sci. Pollut. Res. 21, 4095–4109.

Giang, A., Selin, N.E., 2016. Benefits of mercury controls for the united states. Proc. Nat. Acad. Sci. 113, 286–291.

Gustin, M.S., Amos, H.M., Huang, J., Miller, M.B., Heidecorn, K., 2015. Measuring and modeling mercury in the atmosphere: a critical review. Atmos. Chem. Phys. 15, 5697–5713.

Horowitz, H.M., Jacob, D.J., Zhang, Y., Dibble, T.S., Slemr, F., Amos, H.M., Schmidt, J. A., Corbitt, E.S., Marais, E.A., Sunderland, E.M., 2017. A new mechanism for atmospheric mercury redox chemistry: implications for the global mercury budget. Atmos. Chem. Phys. 17, 6353–6371.

Hu, X.F., Lowe, M., Chan, H.M., 2021. Mercury exposure, cardiovascular disease, and mortality: A systematic review and dose-response meta-analysis. Environmental research 193, 110538.

Hynes, A.J., Donohoue, D.L., Goodsite, M.E., Hedgecock, I.M., 2009. Our current understanding of major chemical and physical processes affecting mercury dynamics in the atmosphere and at the air-water/terrestrial interfaces. In: Mercury fate and transport in the global atmosphere: Emissions, measurements and models, pp. 427–457.

Jung, G., Hedgecock, I.M., Pirrone, N., 2009. ECHMERIT v1.0 – a new global fully coupled mercury-chemistry and transport model. Geosci. Model Dev. 2, 175–195.

Knightes, C.D., Sunderland, E.M., Barber, M.C., Johnston, J.M., Ambrose Jr, R.B., 2009. Application of ecosystem-scale fate and bioaccumulation models to predict fish mercury response times to changes in atmospheric deposition. Environmental Toxicology and Chemistry: An International Journal 28, 881–893.

Kwon, S.Y., Selin, N.E., 2016. Uncertainties in atmospheric mercury modeling for policy evaluation. Current Pollution Reports 2, 103–114.

Lavoie, R.A., Bouffard, A., Maranger, R., Amyot, M., 2018. Mercury transport and human exposure from global marine fisheries. Scientific Reports 8, 6705.

Lelieveld, J., Berresheim, H., Borrmann, S., Crutzen, P.J., Dentener, F., Fischer, H., Feichter, J., Flatau, P., Heland, J., Holzinger, R., et al., 2002. Global air pollution crossroads over the mediterranean. Science 298, 794–799.

Mason, R.P., Choi, A.L., Fitzgerald, W.F., Hammerschmidt, C.R., Lamborg, C.H., Soerensen, A.L., Sunderland, E.M., 2012. Mercury biogeochemical cycling in the ocean and policy implications. Environmental research 119, 101–117.

Mergler, D., Anderson, H.A., Chan, L.H.M., Mahaffey, K.R., Murray, M., Sakamoto, M., Stern, A.H., 2007. Methylmercury exposure and health effects in humans: a worldwide concern. AMBIO: A Journal of the Human Environment 36, 3–11.

Mudelsee, M., 2014. Climate Time Series Analysis: Classical Statistical and Bootstrap Methods, 2nd Edition. Springer.

Mudelsee, M., 2019. Trend analysis of climate time series: A review of methods. Earth-science reviews 190, 310–322.

Muntean, M., Janssens-Maenhout, G., Song, S., Giang, A., Selin, N.E., Zhong, H., Zhao, Y., Olivier, J.G., Guizzardi, D., Crippa, M., et al., 2018. Evaluating edgarv4. tox2 speciated mercury emissions ex-post scenarios and their impacts on modelled global and regional wet deposition patterns. Atmos. Environ. 184, 56–68.

Muntean, M., Janssens-Maenhout, G., Song, S., Selin, N.E., Olivier, J.G., Guizzardi, D., Maas, R., Dentener, F., 2014. Trend analysis from 1970 to 2008 and model evaluation of edgarv4 global gridded anthropogenic mercury emissions. Sci. Total Environ. 494, 337–350.

Munthe, J., Kindbom, K., Parsmo, R., Yaramenka, K., 2019. Technical background report to the global mercury assessment 2018.

Pirrone, N., Cinnirella, S., Feng, X., Finkelman, R.B., Friedli, H.R., Leaner, J., Mason, R., Mukherjee, A.B., Stracher, G.B., Streets, D., et al., 2010. Global mercury emissions to the atmosphere from anthropogenic and natural sources. Atmos. Chem. Phys. 10, 5951–5964.

Pirrone, N., Cinnirella, S., Sprovieri, F., Hedgecock, I.M., D'Amore, F., Bencardino, M., De Simone, F., 2022. The global observation system for mercury (gos 4 m) earth observation applications for the minamata convention on mercury. Earth Observation Applications and Global Policy Frameworks 177–186.

Roeckner, E., Bäuml, G., Bonaventura, L., Brokopf, R., Esch, M., Giorgetta, M., Hagemann, S., Kirchner, I., Kornblueh, L., Manzini, E., et al., 2003. The atmospheric general circulation model echam 5. part i: Model description.

Schartup, A.T., Thackray, C.P., Qureshi, A., Dassuncao, C., Gillespie, K., Hanke, A., Sunderland, E.M., 2019. Climate change and overfishing increase neurotoxicant in marine predators. Nature 572, 648–650.

Scheuhammer, A.M., Meyer, M.W., Sandheinrich, M.B., Murray, M.W., 2007. Effects of environmental methylmercury on the health of wild birds, mammals, and fish. AMBIO: a Journal of the Human Environment 36, 12–19.

Selin, N.E., Jacob, D.J., Yantosca, R.M., Strode, S., Jaeglé, L., Sunderland, E.M., 2008. Global 3-d land-ocean-atmosphere model for mercury: Present-day versus preindustrial cycles and anthropogenic enrichment factors for deposition. Global biogeochemical cycles 22.

Selin, N.E., Sunderland, E.M., Knightes, C.D., Mason, R.P., 2010. Sources of mercury exposure for us seafood consumers: implications for policy. Environmental health perspectives 118, 137–143.

Sheehan, M.C., Burke, T.A., Navas-Acien, A., Breysse, P.N., McGready, J., Fox, M.A., 2014. Global methylmercury exposure from seafood consumption and risk of developmental neurotoxicity: a systematic review. Bull. World Health Organ. 92, 254–269F.

Sprovieri, F., Pirrone, N., Bencardino, M., d'Amore, F., Angot, H., Barbante, C., Brunke, E.G., Arcega-Cabrera, F., Cairns, W., Comero, S., et al., 2017. Five-year records of mercury wet deposition flux at gmos sites in the northern and southern hemispheres. Atmos. Chem. Phys. 17, 2689–2708.

Sprovieri, F., Pirrone, N., Bencardino, M., D'amore, F., Carbone, F., Cinnirella, S., Mannarino, V., Landis, M., Ebinghaus, R., Weigelt, A., et al., 2016. Atmospheric

mercury concentrations observed at ground-based monitoring sites globally distributed in the framework of the gmos network. Atmos. Chem. Phys. 16, 11915–11935.
Steenhuisen, F., Wilson, S., 2022. Geospatially distributed (gridded) global mercury emissions to air from anthropogenic sources in 2015. Atmos. Environ. 211, 138–150.
Streets, D.G., Horowitz, H.M., Lu, Z., Levin, L., Thackray, C.P., Sunderland, E.M., 2019. Global and regional trends in mercury emissions and concentrations, 2010–2015. Atmospheric environment 201, 417–427.
Sun, P., Song, Z., Qin, Y., Xu, Z., Zhang, Y., Zhong, S., Yu, J., 2024. Declines of gaseous element mercury concentrations at an urban site in eastern china caused by reductions of anthropogenic emission. Atmos. Environ. 317, 120199.
Sunderland, E.M., Mason, R.P., 2007. Human impacts on open ocean mercury concentrations. In: Global biogeochemical cycles 21.
Tesán-Onrubia, J.A., Heimbürger-Boavida, L.E., Dufour, A., Harmelin-Vivien, M., García-Arévalo, I., Knoery, J., Thomas, B., Carlotti, F., Tedetti, M., Bănaru, D., 2023. Bioconcentration, bioaccumulation and biomagnification of mercury in plankton of the mediterranean sea. Mar. Pollut. Bull. 194, 115439.
Travnikov, O., Angot, H., Artaxo, P., Bencardino, M., Bieser, J., d'Amore, F., Dastoor, A., De Simone, F., Diéguez, M.d.C., Dommergue, A., et al., 2017. Multi-model study of mercury dispersion in the atmosphere: atmospheric processes and model evaluation. Atmos. Chem. Phys. 17, 5271–5295.
Travnikov, O., Dastoor, A., Friedman, C., Ryzhkov, A., Selin, N., Song, S., 2015. Global mercury modelling: Update of modelling results in the global mercury assessment 2013. Mercury Air Transport and Fate Research.
Van Der Werf, G.R., Randerson, J.T., Giglio, L., Van Leeuwen, T.T., Chen, Y., Rogers, B. M., Mu, M., Van Marle, M.J., Morton, D.C., Collatz, G.J., et al., 2017. Global fire emissions estimates during 1997–2016. Earth Syst. Sci. Data 9, 697–720.
Wu, Q., Tang, Y., Wang, S., Li, L., Deng, K., Tang, G., Liu, K., Ding, D., Zhang, H., 2020. Developing a statistical model to explain the observed decline of atmospheric mercury. Atmos. Environ. 243, 117868.
Zhang, H., Feng, X., Larssen, T., Qiu, G., Vogt, R.D., 2010. In inland china, rice, rather than fish, is the major pathway for methylmercury exposure. Environ. Health Perspect. 118, 1183–1188.
Zhang, H., Holmes, C., Wu, S., 2016. Impacts of changes in climate, land use and land cover on atmospheric mercury. Atmos. Environ. 141, 230–244.
Zhang, Y., Soerensen, A.L., Schartup, A.T., Sunderland, E.M., 2020. A global model for methylmercury formation and uptake at the base of marine food webs. Global Biogeochem. Cycles 34 e2019GB006348.
Zhang, Y., Song, Z., Huang, S., Zhang, P., Peng, Y., Wu, P., Gu, J., Dutkiewicz, S., Zhang, H., Wu, S., et al., 2021. Global health effects of future atmospheric mercury emissions. Nat. Commun. 12, 3035.
Zhou, J., Obrist, D., Dastoor, A., Jiskra, M., Ryjkov, A., 2021. Vegetation uptake of mercury and impacts on global cycling. Nat. Rev. Earth Environ. 2, 269–284.